Artificial Muscle Technology: Physical Principles and Naval Prospects

John D. W. Madden, *Member, IEEE*, Nathan A. Vandesteeg, Patrick A. Anquetil, Peter G. A. Madden, Arash Takshi, Rachel Z. Pytel, Serge R. Lafontaine, Paul A. Wieringa, and Ian W. Hunter

***Abstract*—The increasing understanding of the advantages offered by fish and insect-like locomotion is creating a demand for muscle-like materials capable of mimicking nature's mechanisms. Actuator materials that employ voltage, field, light, or temperature driven dimensional changes to produce forces and displacements are suggesting new approaches to propulsion and maneuverability. Fundamental properties of these new materials are presented, and examples of potential undersea applications are examined in order to assist those involved in device design and in actuator research to evaluate the current status and the developing potential of these artificial muscle technologies. Technologies described are based on newly explored materials developed over the past decade, and also on older materials whose properties are not widely known. The materials are dielectric elastomers, ferroelectric polymers, liquid crystal elastomers, thermal and ferroelectric shape memory alloys, ionic polymer/metal composites, conducting polymers, and carbon nanotubes. Relative merits and challenges associated with the artificial muscle technologies are elucidated in two case studies. A summary table provides a quick guide to all technologies that are discussed.**

***Index Terms*—Actuators, electroactive polymers, shape memory alloys.**

I. Introduction

ELECTRIC motors and combustion engines are relied upon for propulsion, lifting, rotation, positioning, and the application of pressure. Piezoelectric materials complement these actuator technologies by enabling very fine positioning at high frequencies. What is lacking is an established artificial technology that has properties similar to muscle. The properties of number of actuators are presented that are addressing this need.

Why mimic muscle? There are no actuators that can routinely replace muscle when it fails or assist it where it is weak. A muscle-like technology would be of enormous benefit for medical implants and human assist devices, as well as for minimally invasive surgical and diagnostic tools. Combustion engines and high revving electric motors feature high specific power [1] but require complex transmission systems to perform discontinuous and nonrepetitive tasks, greatly reducing their efficiency and increasing cost. Direct drive electric motors are low in force and torque to mass compared to muscle [1]. These deficiencies make human motion and dexterity challenging to reproduce in robots, toys and medical devices. For example, the walking speed of Honda's impressive humanoid robot, Asimo,[1] is limited to 2 km/h by the torque available in the direct drive motors actuating each joint. Biologically inspired hydrodynamic propulsion and maneuvering strategies are also challenging to reproduce using traditional actuator technologies. The availability of a muscle-like actuator will enable important advances in a number of fields.

This review begins with a description of a number of actuator technologies in sequence. All technologies involve materials that change dimensions in response to input electrical, thermal, or optical power. Fundamental mechanisms, basic properties, synthesis, fabrication, and applications are presented. For each material a table of properties is presented. Some of the key figures of merit that are employed are now described.

Stress is the typical force per cross-sectional area under which the actuator materials are tested, and *peak stress* is the maximum force per cross-sectional area under which a material is able to maintain position (also known as blocking stress). In all the actuator technologies described, force developed scales linearly with cross-sectional area (whose surface normal is parallel to the direction in which actuation is occurring).

Strain represents the displacement normalized by the original material length in the direction of actuation. Typical strain is the strain that is often used in working devices, whereas *peak or max strain* is the maximum strain reported. The peak strain generally cannot be obtained when operating at peak stress.

Strain rate is the average change in strain per unit time during an actuator stroke. Typically the maximum reported rate is given. The maximum strain rate is usually observed at high frequencies where strains are small. *Bandwidth* is also discussed for some actuators, and is taken as the frequency at which strain drops to half of its low frequency amplitude. The highest observed frequencies are also mentioned. These may be of interest for acoustic applications. Limitations on bandwidth and strain rate can result from a range of factors including speed of delivery of the input energy (e.g., RC charging time), rates of diffusion or heating, internal dissipation, inertia related effects including speed of sound, and kinetics associated with the energy transduction method [43], [45]. Faster responses can often be obtained by optimizing geometry and processing, and thus the numbers provided are often not ultimate limits but rather represent the current state of the art.

Manuscript received October 23, 2003. This work was supported in part by the U.S. Office of Naval Research under Grant N00014-1-02-0078.

J. D. W. Madden, A. Takshi, and P. A. Wierenga are with the University of British Columbia, Vancouver, BC V6T 1Z4, Canada (e-mail: jmadden@ece.ubc.ca).

N. A. Vandesteeg, P. A. Anquetil, R. Z. Pytel, S. R. Lafontaine, and I. W. Hunter are with the BioInstrumentation Laboratory, Massachusetts Institute of Technology, Cambridge, MA 02139 USA.

P. G. A. Madden is with the Department of Organismic and Evolutionary Biology, Harvard University, Cambridge, MA 02138 USA.

Digital Object Identifier 10.1109/JOE.2004.833135

[1]Honda Motor Company, http://world.honda.com/ASIMO/P3/spec/

Work density is the amount of work generated in one actuator cycle normalized by actuator volume. It is very important to note that this does not include the volume occupied by electrolytes, counter electrodes, power supplies, or packaging, unless otherwise stated. These additional contributions to actuator volume do not always scale linearly with work output and therefore need to be considered separately. Also it is emphasized that the work density is not simply the product of peak stress and peak strain.

Specific power or *power to mass ratio* is the power output per unit mass of actuator material. Typically only the mass of the material itself is considered. Peak power density can be found from the maximum product of simultaneously measured stress and strain rate divided by density. Because of the interdependence of load and rate, peak power is in general less than the product of peak stress and peak strain rate normalized by density.

Efficiency is the ratio of work generated to input energy expended. The listed efficiency has not always been achieved in practice, and sometimes requires additional circuitry to attain. Stored electrical energy and even thermal energy can in principle be recovered in order to improve efficiency.

Electromechanical coupling refers to the proportion of input energy that is transformed into work, including external work done by the actuator and stored internal mechanical energy generated in the actuator itself. The values represent a best case. The coupling values listed here for ferroelectric polymers, dielectric elastomers, and carbon nanotubes represent the ratio of mechanical energy stored within these materials upon actuation under zero load to the electrical input energy [71]. In these cases the most energy that can be extracted to a matched spring is half of the electromechanical coupling ratio.

The coupling is not necessarily the same as the efficiency. In fact in a number of actuators the efficiency can be much higher than the coupling because input electrical or thermal energy can be recovered. Several of the actuator technologies respond as capacitors, for example, from which electrical energy can be retrieved. The coupling is nevertheless important as it indicates how much energy in excess of the energy being converted to work must be shunted back and forth between the power supply and the actuator.

Cycle life is the number of useful strokes that the material is known to be able to undergo. Cycle life is often highly strain and stress dependent. Frequency dependence can arise due to dissipation and heating.

Elastic modulus is the material stiffness multiplied by sample length and divided by cross-sectional area. Generally it is the instantaneous value that is reported, before any creep is induced. It is important as it determines the actuator's passive ability to reject load changes and disturbances, and along with the density and mass determines the frequency beyond which inertial effects become important. Once inertial forces become significant resonance may occur, and at still higher frequencies strains will decrease (typically with the inverse square of frequency).

Many of the materials discussed dissipate mechanical energy, resulting in heating and the damping of mechanical oscillations. Creep and stress relaxation are also important. These effects are seldom characterized and thus are not reported here.

Some materials change stiffness with changing phase or state. Mammalian skeletal muscle changes its stiffness by a factor of 50 [2], for example, a property that is used extensively to assist in control.

Voltage: Most of the technologies described are activated using electrical energy, which serves both to power and control the work that they generate. The *charge density* transferred, and the *dielectric constant* are also important properties.

A number of other properties are often necessary to describe actuating materials including temperature dependence of the response, coefficient of thermal expansion, thermal diffusivity, ionic diffusion coefficients, resistivity, minimum displacement, positioning resolution, and gauge factor. Also environmental resistance can be important in many applications. Unfortunately these characteristics are often not known, or are not included in order to maintain a compact presentation.

The paper concludes with two case studies presenting basic design calculations relevant to the use of artificial muscle technologies to vary propeller blade camber (static) and to increase thrust by generating unsteady flow conditions. A table summarizing properties of all the actuator technologies is also provided.

Previous reviews include a chapter describing classical actuator technologies (electromagnetic actuators, combustion engines, hydraulics, piezoceramics, muscle) by Hollerbach *et al.* [1]. A review of emerging actuator technologies in comparison with muscle written by Hunter and Lafontaine over a decade ago remains relevant [2]. A book with chapters describing in detail many of the technologies presented here, edited by Bar-Cohen, provides a comprehensive introduction [3]. Bar-Cohen also hosts an informative Web site devoted to electroactive polymer actuators and devices.[2] The proceedings of the SPIE annual Smart Structures and Materials Symposium feature sessions on electroactive polymers, ferroelectrics, and ferroelectric shape memory alloys. Papers by Ashby and colleagues describe methods used to create a database of actuator properties [4].

A number of interesting actuator technologies have been omitted from this review. For example, single crystal ferroelectrics such as PZN-PT and PMN-PT are similar to traditional piezoceramic actuators in many respects, but feature significantly larger strains ($\sim$1%). These materials are now commercially available and relatively established. In this paper new larger strain polymer-based ferroelectrics are discussed. Shape memory polymers undergo large thermally induced deformations ($>$100% strain) [5]. Like heat shrink tubing these generally need to be retrained after one actuation cycle. Polymer gels (e.g., polyacrylonitrile [6]) undergo large deformations in response to changes in temperature, pH or solvent environment. These materials can reversibly actuate over many cycles with strains of greater than 100%. Traditionally gels have been slow to respond (seconds to minutes), are relatively weak ($\sim$100 kPa), and are low in efficiency, and therefore have not been discussed in detail here. Electrostatic actuators are

[2]http://eap.jpl.nasa.gov/

TABLE I
MAMMALIAN SKELETAL MUSCLE [2], [7]

PROPERTY	TYPICAL	MAXIMUM
Strain (%)	20	> 40
Stress (MPa)	0.1 (sustainable)	0.35
Work Density ($kJ \cdot m^{-3}$)	8	40
Density ($kg \cdot m^{-3}$)	1037	
Strain Rate ($\%\cdot s^{-1}$)		> 50
Specific Power ($W \cdot kg^{-1}$)	50	284
Efficiency (%)		40
Cycle Life		$> 10^9$
Modulus (MPa)	10 - 60	

being applied to microelectromechanical systems.[3] These employ electrostatic attraction between microfabricated electrodes in order to generate forces and displacements. Electrostatic actuators are capable of relatively large strains (>50%) at low stress (~10 kPa) and moderate to high bandwidth (>100 Hz). Electrostatic actuators are based on fabricated structures rather than field induced changes in mechanical properties and have been omitted.

II. ACTUATOR DESCRIPTIONS

A. Muscle and Biological Actuators (Table I)

Muscle is a linear actuator technology whose properties, though surpassed in many respects by artificial actuators, are very well suited to providing intermittent displacements and adaptable stiffnesses in organisms ranging from micrometers to meters in length. Details of the mechanisms are provided by Kohl as part of this special issue. The properties vary by species, as described by Full and Meijer [7]. Key characteristics of mammalian skeletal muscle are provided in Table I for ready comparison with other technologies [2].

As mentioned, muscle does not surpass artificial actuators in any one aspect (for example continuous power to mass is an order of magnitude lower than that of an internal combustion engine). However there are a number of attractive design features that could be emulated to great advantage. For example, force can be graded by controlling the number of fibers that are activated in parallel, a process known as recruitment. This grading of force enables efficiency to be optimized over a wide range of loads and contraction velocities, in addition enabling control of acceleration and force. The control of force is made more effective by the fact that inactive muscle fibers are relatively low in stiffness, and therefore do not require significant forces to strain. In most of the materials described below there is little ability to change modulus. As a result attempts to grade force by recruitment are less effective. The ability to change stiffness is also important in control strategies. For example, in catching a ball, too stiff an arm will lead to a large (painful) impulse as the ball makes contact, and provides less time to grasp the ball before it bounces back. A very compliant arm will not be able to stop the ball. The optimum stiffness needs to be adapted to the ball mass and velocity. Such stiffness control can be emulated in artificial actuators by fast feedback control, but at the expense of added complexity and will only work if the actuator bandwidth is sufficient.

A further advantage of muscle is its ability to convert chemical energy to mechanical work. The "combustion" of sugars and fats using freely available oxygen provides a fuel energy density that is two orders of magnitude greater than that of batteries. Most of the actuator technologies described below require electrical energy and will generally rely on batteries when used in autonomous systems such as autonomous underwater vehicles (AUVs). Improvement in the cost, energy density, and cycle life of fuel cells will alleviate this issue in systems that have access to air. Submersible use is more challenging as both fuel cells and chemical oxidation reactions require the harvesting of dissolved oxygen and of air bubbles, or oxygen must be carried.

Another attractive characteristic of muscle is its integrated circulation system, which delivers fuel (glucose and oxygen), and removes heat and waste. Capillary density is such that molecules and heat need only diffuse over distances of some tens of micrometers. Such local delivery of energy and removal of heat could greatly benefit a number of artificial actuators in which it is desirable to rapidly transfer heat, mass and energy.

Finally, muscle is able to operate for billions of cycles over a period of a hundred years or more. This exceptional performance is made possible by the ability to regenerate proteins in situ.

Many of muscle's advantages relative to artificial actuator technologies stem from nature's ability to fabricate and control on length scales ranging from the molecular to the macroscopic. As fabrication technology improves and nature's mechanisms are better understood, a number of muscle's properties, including regeneration, nanostructuring and direct chemical actuation, will likely become common in artificial actuators. Nevertheless, some artificial actuator technologies are already matching or exceeding muscle in strain, stress, and specific power, and are thus worthy of attention. Most of the technologies presented, for example, feature peak stresses that can at least match muscle, with the peak forces per cross-sectional area in shape memory alloys exceeding those of muscle by a factor of 500. Furthermore, unlike mammalian skeletal muscle, nearly all of the technologies presented feature a "catch" state, enabling position to be locked against a fixed load without power expenditure.

B. Dielectric Elastomer Actuators (Table II)

Electrostatic attraction between conductive layers applied to two surfaces of elastomer films induces compressive strains under applied fields of ~150 MV/m, as depicted in Fig. 1 [8]–[16]. Elastomers are sufficiently compliant that large strains are induced and there is efficient coupling between the electrical energy input and mechanical energy output. Typically the spacing between conductive layers is less than 0.1 mm, so that although strains are large, total displacement is small. Since elastomers maintain constant volume, contraction in one direction leads to expansion in the other two. Most mechanisms make use of the expansion perpendicular to the direction of the applied field because these result in large displacements. By prestraining one of the two axes most of the expansion is

[3]http://www.analog.com/

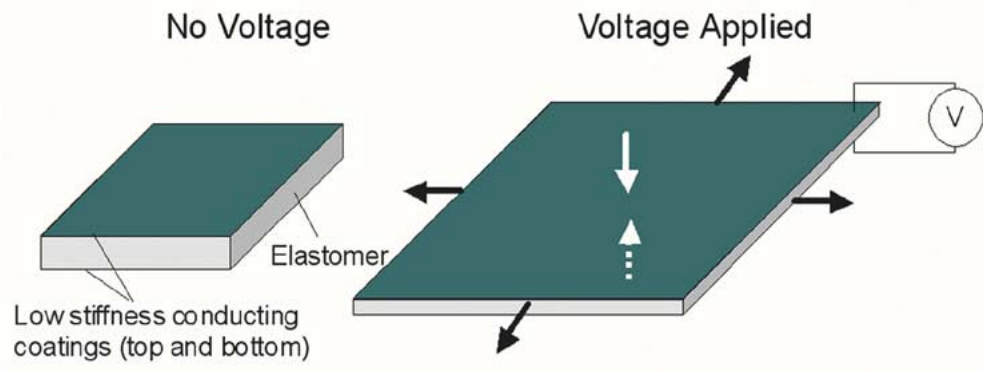

Fig. 1. Diagram depicting the effect of applied voltage on a slab of dielectric elastomer. (Adapted from Kornbluh *et al.* [9].)

TABLE II
DIELECTRIC ELASTOMERS [9]–[15], [17]

PROPERTY	SILICONE	VHB
Maximum Strain (%)	120	380
Stress (MPa)	0.3 typical 3.2 max	1.6 typical 7.7 max
Work Density (kJ/m^3) (Based on internal strain)	10 typical 750 max [20]	150 typical 3400 max [20]
Density (kg/m^3)	1100	960
Peak Strain Rate (%/s) *-Achieved at:* -Modified VHB [20]:	34,000 *12%, 1400 Hz*	450 *2.3%, 100 Hz* 4500
Peak Power (W/kg) *Taken at Peak Rate w/ load of*	5,000 *300 kPa*	3,600 *1.6 MPa*
Continuous Power (W/kg)	500	400
Bandwidth (Hz) - 3 dB: - maximum observed freq:	1400 > 50 kHz	10 (100 [20]) > 50 kHz
Life (cycles) @ strain > indicates no failure observed	>10^7 @ 5% 10^6 @ 10%	>10^7 @ 5% 10^6 @ 50%
EM Coupling (%) ≅ strain, for small strains [20]	80 max 15 typical	90 max 25 typical
Efficiency (%) (conversion to internal strain)	80 max 25 typical	90 max 30 typical
Modulus (MPa) (process and strain dependent)	0.1 to 1.0	1.0 to 3.0
Speed of Sound (m/s)	< 30	< 55
Thermal Expansion (m/m/°C)		$1.80 \cdot 10^{-4}$
Voltage (V) (Geometry dependent)	> 1000	> 1000
Dielectric constant @ 1 kHz	~ 3	~ 4.8
Max. Field (MV/m)	110 - 350	125 - 440
Temperature range (°C)	-100 to 250	-10 to 90

directed perpendicular to the prestrain [10]. The prestraining can also result in higher breakdown potentials [12].

1) Features: The actuators are elegantly simple in mechanism and construction and feature large strains that are typically in the range of 10% to 100% but can reach 380% [9]–[17]. High efficiencies (>30%) are possible with careful design, particularly when energy is recovered. High bandwidths are achievable in silicone (1400 Hz), and moderate bandwidths are possible in acrylic VHB 4910 from 3M (VHB 10 Hz typical) [9]. Small displacements can be achieved at tens of kilohertz in both materials [9]. These materials can also act as generators and sensors. Finally, dielectric elastomers operate over relatively large temperature ranges. Silicone in particular can operate over a temperature range of -100 to $+250$ °C.

2) Limitations: High voltages (>1 kV) can be a concern, particularly in biomedical and toy applications. For large and fast devices the power may provide a real hazard. Generally there is a need to convert line or battery voltages up to kilovolt potentials, which adds cost and consumes volume. Relatively small dc–dc converters are available for moderate to low power applications (e.g., cubes 12.7 mm on each side from EMCO High Voltage), but the cost and size at present are prohibitive for application in small (e.g., handheld) portable devices [11]. Dielectric breakdown can limit actuator yield especially when imperfections exist within films. The materials themselves can actuate at high stresses (up to 7.7 MPa in acrylic and 3.2 MPa in silicone). However, in practical devices the maximum stress is typically an order of magnitude lower due to the reduced electric field required to avoid premature breakdown and to imperfect mechanical coupling with the load. Finally, the mechanisms needed to apply prestrain add significantly to volume and mass [11].

3) Theory: The stress or pressure P_z resulting from electrostatic attraction between plates is

$$P_z = \varepsilon_r \varepsilon_0 E^2 = \varepsilon_r \varepsilon_0 (V/t)^2 \tag{1}$$

where ε_r is relative permittivity (dielectric constant), ε_0 is the free space permittivity, E is the applied electric field, V is the applied voltage, and t is the thickness of the polymer. The maximum stress is limited by dielectric breakdown, which in turn is a function of strain.

In attempting to fully model this apparently simple system several complications arise. The resultant strains produced in the polymer are dependent on the boundary conditions and loads on the polymers. Further, the strain depends on the elastic modulus of the polymer, which is nonlinear at large strains. The large prestrains used can cause the effective elastic modulus to be anisotropic. However by assuming that the elastomer is incompressible, the strains S in the x, y, and z directions obey a simple relationship

$$(1 + \mathrm{S_x})(1 + \mathrm{S_y})(1 + \mathrm{S_z}) = 1. \tag{2}$$

S is the relative strain, which is the strain difference from prestrain conditions.

4) Materials and Dimensions: A number of elastomers have been tested, with the best results achieved from three commercially available materials, namely, Dow Corning HS3 silicone, Nusil CF 19-2186 silicone, and 3M VHB 4910 acrylic. The silicones are cast into the desired geometries, while the VHB is purchased as an adhesive ribbon. Typical actuator dimensions before stretching are 100 μm thick, 100 mm long, and similar dimensions in width. These films are coated with conductive grease, powder or paint. Prestretching of up to 500% is performed by rolling films, inserting them into a compliant frame, or by using beams to maintain the tension [9]–[16]. Voltage is applied to either side at potentials of up to $\sim$10 kV and using currents in the milliamp range.

5) Devices and Applications: Recently "spring roll" actuators have been developed that feature up to three degrees of freedom each [11]. These actuators have a helical spring at their core, around which dielectric elastomer sheet is wound. The sheets are coated with electrodes. In order to produce bending motions (in addition to stretching along the axis) the electrodes are patterned such that voltage can be applied independently to each of four sections. The resulting actuator bends in two directions and extends. This mechanism is very similar to that used in piezoceramic tube actuators, but features much larger deflections. These tubes can generate up to 30 N of force or 20 mm of displacement from a 90 mm long, 18 mm diameter device. The effective stress is 0.1 MPa, and the strain is 22%.

Demonstration devices include speakers (tweeters), pumps, and multilegged robots [14].

6) Rate Limiting Mechanisms: RC charging, viscoelastic behavior, inertia, dissipation induced heating, and the speed of sound are all rate limiting factors [9]. Interestingly the VHB based actuators exhibit a frequency response that is two orders of magnitude lower than observed in silicone [9].

7) Temperature: Dielectric elastomers have been operated successfully between 250 °C, and at -100 °C for silicones and -10 °C and 90 °C for acrylic [11]. Operation below glass transition temperatures will be ineffective as the compliance will drop by two or more orders of magnitude. Nevertheless, the temperature range is impressive, especially when compared to relaxor ferroelectrics.

8) Potential: Layers of thin films could enable voltage to be substantially reduced. Ideally these layers would be as thin as 100 nm, reducing potentials to the 10 V range. However this may prove difficult if even moderate strain rates are to be achieved due to the conflicting requirements of maximizing the conductivity of the electrodes and minimizing their mechanical stiffness. Increasing dielectric constant is an alternative method for reducing applied voltages, as predicted by (1). It may be possible to devise composite materials with high dielectric constants and moderate breakdown potentials that enable low voltage operation without sacrificing performance.

C. Relaxor Ferroelectric Polymer Actuators (Table III)

1) Mechanisms: Ferroelectric materials are the electrostatic analogs of ferromagnets. The application of an electric field aligns polarized domains within the material. When the applied field is removed, a permanent polarization remains. As in ferromagnets, ferroelectrics are characterized by a Curie point, a temperature above which thermal energy disrupts permanent polarization.

TABLE III
FERROELECTRIC POLYMERS [20], [24], [26]

PROPERTY	TYPICAL	MAXIMUM
Strain (%)	3.5	7
Stress (MPa)	20	45
Work Density (kJ/m^3) (based on internal strain)	320	> 1000
Density (kg/m^3)	1870	2000
Strain Rate (%/s)		≥ 2000 *10 kHz, ~0.1% strain*
Bandwidth (Hz)	< 100	> 10,000 *for strain ~ 0.1 %*
EM Coupling S3 (at optimal temperature)	0.1 - 0.2	
EM Coupling S1 (at optimal temperature)	0.4	
Modulus (MPa) (Composition dependent)	400	1200
Voltage (V) (Geometry depen.)		> 1000
Max. Field (MV/m)	13	150
Dielectric Constant varies between ~ 4 & 60.	55	Temp. dependent
Temperature Range	ΔT ~ 60 °C	

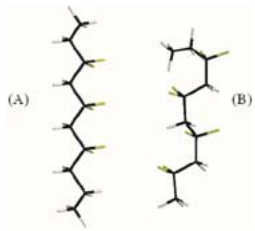

Fig. 2. An example of the molecular shape changes obtained by applying a field to ferroelectrics. A segment of vinylidene fluoride oligomer is shown in two conformations. (A) is a model of the polar all trans conformation that is obtained upon application of a field, while (B) is an alternating trans-gauche form that is nonpolar. The black rods represent the carbon backbone, the green segments are fluorine and the white segments are hydrogen. (Adapted from Xia *et al.* [26].)

The ferroelectric polymer most commonly used for actuation is poly(vinylidene fluoride—trifluoroethylene), abbreviated as P(VDF-TrFE). The electronegativity of fluorine creates local dipoles on the polymer backbone. These polar groups align to create polarized domains within a molecule, as depicted in Fig. 2(A), and across crystalline regions. The application of an electric field aligns polarized domains, which remain even after the field is removed. The realignment also produces reversible conformational changes which are made use of in actuation [26].

A key disadvantage of ferroelectric polymers is that there is substantial hysteresis. A large field must be applied in the opposite direction of the initial field in order to reverse the polarization, and substantial energy is dissipated. The highest performance materials have instead been ferroelectric relaxors in

which the long range correlations between polar groups are disrupted by imperfections. These imperfections are introduced by either irradiation [24] or by the incorporation of disruptive monomers along the chain, such as chlorofluoroethylene [26]. The imperfections are used to bring the Curie point below room temperature, such that a nonpolar, paraelectric phase dominates at normal operating temperatures. An example conformation that is in the paraelectric phase is shown in Fig. 2(B). When field is applied to the polymer in this state polarization is induced, resulting in a conformation similar to that shown in Fig. 2(A). The imperfections introduced into the structure reduce the energy barriers to phase change, thereby reducing or eliminating hysteresis [26]. This ferroelectric to paraelectric transistion is associated with relatively large molecular conformational changes, leading to macroscopic deformations that are employed to generate actuation.

In P(VDF-TrFE) ferroelectric relaxors, application of field leads to a contraction in the direction between plates (S3), and extension perpendicular to the applied field (S1, S2). Prestretching the polymers—e.g., along S2—enlarges the strain in this direction due to alignment of molecules in the stretch direction [26].

2) Features [18]–[26]: Moderate strains are achieved (up to 7%), with high stresses (reaching 45 MPa), moderate to excellent frequency response (deflections are observed at up to ~100 kHz), large work per cycle (approaching 1 MJ · m^{-3}), and high stiffness (>0.4 GPa depending on the density of imperfections) [20], [24], [26]. The work densities reported for ferroelectrics and dielectric elastomers are based on internal strain, as discussed in the introduction, and at best half of the energy will be extracted to a perfectly matched load. Nevertheless the work density is impressive.

3) Limitations: These actuators, like dielectric elastomers, require high fields (~150 MV · m^{-1} and voltages (>1 kV). Electrodes applied to the surface of the polymer fatigue due to the large strains imposed. Dissipation and the associated heating of the actuators often make the achievement of frequencies above 100 Hz impractical except in small samples or at small strains.

Some of the fluorocarbons used in the synthesis of the materials are difficult to obtain and expensive due to environmental restrictions on their use. The process of e-beam irradiation, used in a number of the materials, is expensive and time consuming. However the methods for polymerizing poly(vinylidene fluoride—trifluoroethylene) itself [23] are similar to those used to create polyethylene, and are therefore readily scaleable and low cost.

These materials feature an optimal loading condition at which maximum strain is achieved. Above and below this value, strain decreases substantially. For example in irradiated P(VDF-TrFE) the peak strain occurs at 20 MPa, dropping to ~50% of its peak value above 40 MPa and below 5 MPa [26].

4) Potential: The high voltages can be reduced by using thin layers (100 nm for 15 V) or by creating materials with very high dielectric constants. The relative stiffness of the electrode materials limits the extent by which film thickness and hence applied voltage can be reduced, a limitation that might be overcome to some extent by using electrodes that are more compliant than gold and other metals commonly employed. The addition of high dielectric constant filler materials to the polymer matrix is showing promise in greatly reducing the required field strength [18], [21], [26]. The addition of copper phthalocyanine to a P(VDF-TrFE) matrix enabled 2% strain at 13 MV·m^{-1} while maintaining a composite elastic modulus of 0.9 GPa. The reduction in applied field is attributed to an increase in applied dielectric constant from ~50 to >400 [26].

TABLE IV
LIQUID CRYSTAL ELASTOMERS [29], [32], [34], [36], [37]

PROPERTY	THERMAL	E-FIELD [29]	E-FIELD [36]
Strain (%)	19-45	4	2
Stress (MPa) – at max. strain - isometric (no strain)	0.01 – 0.12 typ. 0.45 max.		
Work Density (kJ/m^3)	3 – 56		20 internal
Strain Rate (%/s)	6 - 37	1000	
Power (W/kg)	1		
Efficiency (%) - thermal -conversion to internal strain	< 5 % Carnot		75
Modulus (MPa) at 0 % strain 30 % strain 120 % strain	4 0.06 0.3		100
Voltage (V) (applied to a 75 nm thick film)		0.11	
Max. Field (MV/m)		1.5	25
Dielectric Constant - 0.1 Hz - 100 Hz			15-40 3-5

5) Temperature: The Curie point of many of these materials is just below room temperature. The dielectric constant and the efficiency of coupling electrical and mechanical work is also a function of temperature. The operating temperature range (~60 °C) is dependent on the density of imperfections (introduced either by irradiation or by the concentration of disruptive monomer units). The Curie point and the temperature range of operation can be tuned up or down by changing the density of imperfections. A typical range is between 20 and 80 °C [24].

Heat can be used instead of electrostatic energy to activate ferroelectric polymers [22]. Heating and cooling these polymers around their Curie point produces reversible actuation (<10% strain), with efficiency determined by the Carnot relationship.

6) Rate Limiting Mechanisms: Rates are limited by RC charging times, heating and dissipation within the materials, inertial effects, and ultimately the relaxation times of the polar groups on the backbone.

D. Liquid Crystal Elastomers (LCEs) (Table IV)

Thermal or electrostatic energy are employed to induce phase changes in liquid crystalline polymers [27]–[37]. The changes of order and alignment of liquid crystalline side chains generate stresses in the polymer backbone, resulting in actuation.

1) Mechanisms: In 1975 de Gennes [27] predicted that the reorientation of liquid crystal molecules during a phase transition could lead to a mechanical stress and strain. Stress fields in liquid crystals generally induce flow that prevents the buildup of static forces. In liquid crystal elastomers, the free flow of

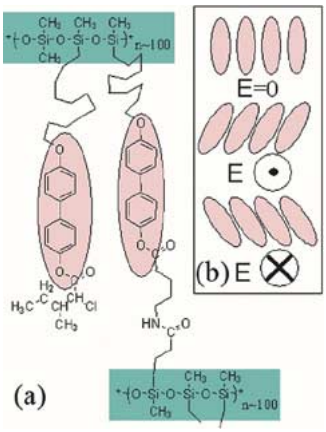

Fig. 3. An example ferroelectric liquid crystal elastomer. (a) The polymer backbone (green square) is siloxane, from which mesogens (ovals) extend. A small fraction of the mesogens are crosslinked to neighboring polymer chains. In the system shown the application of a field normal to the long axis of the mesogens produces a reversible rotation, as depicted in (b), resulting in dimensional changes. (Adapted from Lehmann *et al.* [29].)

the liquid crystal molecules (mesogens) is prevented by bonding them to a cross-linked polymer in which a flexible backbone still allows reorientation of the mesogens, as depicted in Fig. 3(a). The change in orientation of the mesogens upon temperature changes or application of an electric field produces stresses and strains that are transferred via the backbone to perform mechanical work. The mechanisms of field driven actuation in LCEs are similar to those of the ferroelectrics described above, with the exception that the polarized units do not form part of the polymer backbone itself, but rather are appendages extending from it.

Rate is limited by heat transfer time constants when thermally driven. For a step change in temperature applied to the surface of a thin film of material, an estimate of the time constant of the diffusive heat transfer within the polymer itself can be given as

$$\tau = R_{\rm th} \cdot C_{\rm th} = \rho \cdot C_v \cdot L^2 \tag{3}$$

where $R_{\rm th} = \rho \cdot L/A, C_{\rm th} = C_v \cdot L \cdot A$, and ρ is the thermal resistivity, C_v is the volumetric heat capacity, A is the area perpendicular to the heat flow, and L is the distance the heat must diffuse. The quantity $(\rho \cdot C_v)^{-1}$ is known as the thermal diffusivity. Leister *et al.* [30] measured the thermal diffusivity for a ferroelectric liquid crystalline elastomer with a polysiloxane backbone and found values of 2×10^{-8} to 4×10^{-8} m^2/s in 20 to 100 μm thick samples. For a flat film with a thickness of 100 μm, the corresponding time constant is between 0.25 and 0.5 s if heat is transferred on only one side of the film, and less than 0.125 s for both sides. The rate is expected to be proportional to the inverse square of thickness, so it should be possible to activate a 1 μm thick film in less than 100 μs.

Ferroelectric liquid crystals contract and expand when an external electric field is applied to the polymer [29], [36], [37]. The mesogenic units in ferroelectric liquid crystals have an intrinsic polarization or feature an anisotropic dielectric constant [36]. The application of field changes the alignment of the mesogens as depicted in Fig. 3(b), with the direction and extent of reorientation depending on the mesogens used. These reorientations induce bulk stresses and strains.

Unlike thermal energy, electric fields can be applied through the bulk of the material very quickly, so the response speed is considerably faster in electrostatic-driven films than during thermally induced activation. The time taken to reorient the liquid crystal units is the ultimate rate-limiting factor in ferroelectric liquid crystalline elastomers. In experiments designed to determine the speed to the mesogenic reorientation, Skupin *et al.* [33] used time resolved Fourier transform infrared spectroscopy (FTIR) to measure a response time constant of $\sim$10 ms, thus providing a lower limit on the response time of their material. The response time depends greatly on the specific mesogens used, the polymer backbone structure, and the degree of cross-linking, and thus smaller mesogens, in a less cross-linked matrix could be faster (and would likely exhibit less strain).

In separate experiments by the same group [29], 4% electrostrictive strains were observed in a ferroelectric liquid crystalline elastomer at 133 Hz. In these experiments an electric field of 1.5 MV/m was applied to a thin (75 nm) sample. Recent experiments by Huang *et al.* [36] show a 2% strain at 25 MV$\cdot$m^{-1} in a relatively stiff material (100 MPa), with an apparently rapid drop off in frequency response above 1 Hz. The electromechanical conversion efficiency is found to be 75% in this material (conversion is to internal strain in the actuator in this case, and not to external work, as discussed in the introduction).

2) Features: These materials can exhibit good response times ($\sim$10 ms in field driven actuation [29]), and moderate to large strains ($\sim$4% in the field driven materials, and up to 45% in thermally activated polymers). The applied fields (1.5 to 25 MV/m) are significantly lower than those used in other ferroelectrics and in dielectric elastomers, leading to correspondingly lower applied voltages for the same thickness of material.

Thermally driven LCEs can be activated via radiative heating, which can potentially create fast activation, providing that absorption can be made uniform (cooling still relies on thermal conduction and is thus relatively slow in thick samples) [33]. Joule heating of graphite loaded [37] or conducting polymer coated liquid crystal elastomers [35] has also been used to induce actuation.

3) Limitations: Investigation of LCEs is still at a very early stage with the result that much information has yet to be collected. These materials are elastomers with low stiffness and tensile strengths so that a relatively small change in load can easily lead to a large change in length. Thermal activation is limited by Carnot efficiency, and heating must continue during activation periods. The rate of thermal actuation is limited by heat transfer rates. Very fast rates might be achieved using laser heating, but at the cost of further reduced efficiency. The low stiffness of these materials means that resonant frequencies and the speed of sound are low. The use of stiffer materials [36] has so far resulted in lower bandwidths.

E. Conducting Polymer Actuators (Table V)

1) Synonym: Conjugated polymers.

2) Mechanisms: Conducting polymers are electronically conducting organic materials featuring conjugated structures, as depicted in Fig. 4. Electrochemically changing oxidation state leads to the addition or removal of charge from the

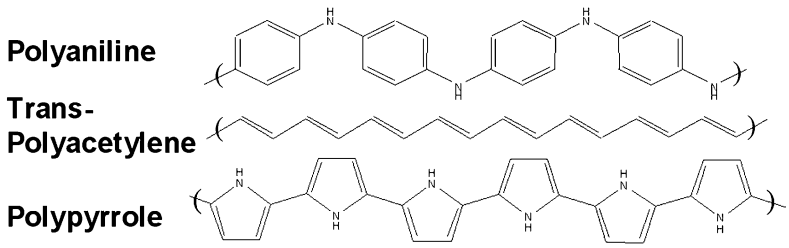

Fig. 4. Structures of three conducting polymers that are employed as actuators.

TABLE V
CONDUCTING POLYMER ACTUATORS

PROPERTY	MIN.	TYP.	MAX.	LIMIT	REFS.
Strain (%)		2	12	> 20	41-44, 60,64
Stress (MPa)		5	34	200	38, 42-45
Work Density (kJ/m^3)		100		1000	38,43
Strain Rate (%/s)		1	12	10,000	46,49
Power (W/kg)			150	100,000	43
Life (cycles)		28,000	800,000		52
Coupling			0.1		45
Efficiency (%)		< 1	18		45
Modulus (GPa)	0.2	0.8	3		43,45,49,52
Tensile Strength (MPa)		30	120	400	38,45
Applied Potential (V)		1.2	10		53
Charge Transfer (C/m^3)	10^7		10^8		43-46
Conductivity (S/m)		10,000	45,000		45,51
Cost (US$/kg)	3		1000		45

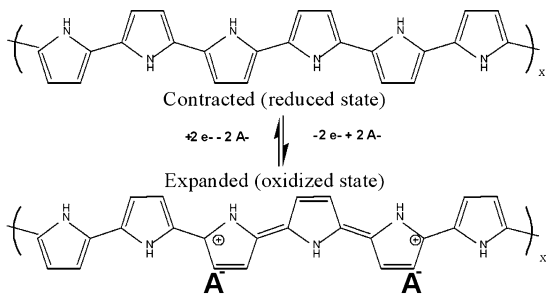

Fig. 5. Conducting polymer actuators undergo dimensional changes in response to changes in oxidation state. In the example shown polypyrrole expands as it is oxidized. Anions (A^-) enter to balance charge as electrons are removed. Expansion is generally correlated with net ion flux into the polymers [39].

polymer backbone and a flux of ions to balance charge, as depicted in Fig. 5. This ion flux, which can be accompanied by solvent, is associated with swelling or contraction of the material [38]–[41]. Insertion of ions between polymer chains appears to be primarily responsible for dimensional changes, although conformational changes of the backbone and solvent flux may also play a role. Changes in dimension can also be chemically triggered [41].

3) Features: High tensile strengths (can reach >100 MPa [38]), large stresses (up to 34 MPa [42]), and stiffnesses (~1 GPa modulus [43]–[45]), combined with low voltages (~2 V [38]–[53], [56]–[58]) make this actuator technology attractive.

4) Limitations: The electromechanical coupling in these materials is often less than 1%, except at small strains [45], [46]. As a result, efficiency is also low unless a substantial portion of the input energy is recovered. A consequence of the low electromechanical coupling and the low activation voltages is that very high currents can be required to operate at high power [43], putting constraints on the power supply, particularly in autonomous applications. Encapsulation issues need to be addressed in order to isolate actuators from the environment [44], [49], [50], [57], [58]. The moderate strains (~2%) require mechanical amplification in many applications [57]. Strain rates are moderate to small (12%/s max to date). Rates are limited by internal resistance of the polymers and electrolytes, and by ionic diffusion rates of ions inside the polymer [43]–[46].

5) Modeling: Experiments show that strain ε is proportional to the density of charge ρ transferred over a range of strains of about 1%

$$\varepsilon = \frac{\sigma}{E} + \alpha \cdot \rho \tag{4}$$

where σ is the applied stress and E is the elastic modulus [38], [40], [41], [44]–[46]. The strain to charge ratio α is approximately ± 1–5×10^{-10} m^3·C^{-1} ([45, p. 42]). The sign of the strain to charge ratio is negative when cations dominate the ion transfer and positive when it is anions that serve to balance charge [39]. The ion that dominates is generally the smallest of the available cations and anions. For larger strains this relationship continues to hold to first order. At stresses of more than several megapascals, effects of creep and stress relaxation begin to become significant, and so the purely elastic relationship between stress and strain, represented by the first term on the right hand side of (3), is no longer adequate [42].

If the strain to charge ratio is expressed in terms of change in volume per ion transferred, the volume corresponds approximately to the size of an ion ([45, p. 103]), but an intercalation model of actuation is likely an oversimplification. In some cases the polymer may exhibit gel-like behavior, where change in oxidation state is associated with large solvent flux, large volume changes, and significant changes in modulus [60].

Rate of actuation is primarily limited by the rate at which charge can be injected. Charge transfer is restricted by the internal resistance of the cell (when electrochemically activated) and by the rate at which ions are transferred within the polymer [43], [46]. Some of the internal resistance can be compensated for by increasing applied potential in a controlled manner, resulting in substantially improved rates of actuation [53],

[49]. The fastest response is predicted to occur in thin films with closely spaced electrodes that employ highly conducting polymer [43].

6) Materials and Dimensions: Polypyrrole and polyaniline are the most widely used materials. There has also been some use of polyacetylenes [48], polythiophenes and polyethyldioxithiophene [56]. Monomers are available (e.g., www.basf.com) for these materials. The most common mode of synthesis is electrodeposition [51], producing thin ($\sim$40 μm thick) films with typical widths of 10 mm and lengths of up to 1 m or more [45]. Samples can also be electrodeposited as tubes [49], or chemically synthesized [41], [50]. The properties of the polymers are very dependent on the solvent and salts used in deposition [51], [59], and also the electrolyte employed during actuation [39], [44], [52], [59]. The cycle life for example can be extended to approximately 1 million cycles from several tens of thousands by using ionic liquid electrolytes [52].

Forces produced by these actuators have reached tens of Newtons with displacements of several millimeters, and use of mechanical amplification increases displacements up to about 100 mm [57]. Voltages of up to 10 V are used to drive currents that reach several hundred milliamperes. Voltages of only 1–2 V are sufficient for activation, but higher voltages help speed the response [53]. At steady state (no motion) current is minimal, even when forces are applied. Thus a catch state is available, with essentially no energy being expended in order to maintain a constant force.

7) Temperature: Little work has been done to characterize the response of conducting polymer actuators under conditions other than room temperature. The conductivities of the polymers are known to be functions of temperature and synthesis conditions [54], [55]. Electrolyte conductivity and ion diffusion rates are anticipated to decrease in proportion to the square root of absolute temperature, thereby affecting rates at low temperatures. Finally, electrolyte freezing will drastically reduce rate. Typical freezing temperatures are between -60 and 0 °C.

8) Applications: Demonstration braille cells [52] and variable camber blades have been built [57]. On the microscale, cell traps and medical devices are being created.[4]

9) Potential: Layers of thin porous films could enable extremely fast, high power response ($>$100 kW/kg) [43], [45], [46]. Recovery of stored electrochemical energy should enable moderate efficiencies to be achieved even at full strain. Recent results in polypyrrole demonstrate strains of 12% under moderate stresses [0.5 (MPa)] [60]. Newly designed conducting polymers promise larger strains and higher electromechanical coupling, but are still at an early stage of development (see next section).

Data and models valuable to engineering design of conducting polymer actuators, and particularly polypyrrole based actuators, are provided by Madden [43], [46], while a discussion of current status, promise and remaining challenges is given by Smela [59]. A paper by Madden *et al.* in this issue reviews practical considerations associated with the application of conducting polymer actuators.

[4]http://www.micromuscle.com

F. Polymeric Molecular Actuators

Muscle employs individual chemically driven molecular conformational changes to produce macroscopic deformation and forces. Synthetic chemistry has produced a number of interesting actuating molecules that contract, slide, rotate, and ratchet on the molecular scale [61]–[63]. Polymeric molecular actuators attempt to harness such molecular interactions on larger scales by linking together many active components into a macromolecule, as depicted in Fig. 6. Actuation is achieved by chemically or electrochemically modifying bonds along polymer chains and between chains to induce conformational changes [64], [67], [68]. Photoinduced changes are also employed [61], [69]. These technologies are at an early stage of research. Two approaches are briefly discussed.

1) Mechanisms: Molecular conformational changes are induced in materials designed to utilize a variety of mechanisms such as *cis-trans* photoactivated transitions, molecular bending due to changes in hybridization and $\pi-\pi$ molecular dimerization [61], [64]–[69]. In principle, the molecular structural changes are designed in order to maximize mechanical performance.

2) Example: Poly(Calix[4]Arene Bis-Bithiophene): Poly(calix[4]arene bis-bithiophene) [poly(CalixBBT)] employs hinge molecules (calix[4]arene) interconnected by rigid rods (quarterthiophene). The rods attract one another in the oxidized state, contracting the material into a folded molecular structure. This molecular contraction is driven by the $\pi-\pi$ dimerization ($\pi-\pi$ stacking) of thiophene oligomers upon oxidation, which is intended to produce a reversible molecular displacement [64]. The cone conformation of the calix[4]arene scaffold allows generation of an accordion-like molecule upon electrochemical polymerization.

Key features of this material include the deformable calix[4]arene scaffold and the redox active quarterthiophene redox units. The proposed actuation mechanism and a three-dimensional space-filling model are shown conceptually in Fig. 6. The initial polymer displays an equilibrium conformation that has the quarterthiophene groups in a nonaggregated state. Upon oxidation the quarterthiophene groups have a strong tendency to aggregate into π-stacked structure. Inspection of the space-filling model suggests that one-dimensional changes of more than 100% are possible.

The mechanism presented above and referred to as π dimerization or $\pi-\pi$ stacking makes use of wavefunction overlap in π-onjugated polymers. The π-dimerization is attractive in the oxidized state (electron deficient) and repulsive in the reduced state (filled electronic levels) [65], [66].

It is hoped that these materials will overcome two limitations of conducting polymer actuators, namely, the limited strain and the low degree electromechanical coupling, while maintaining the advantage of low voltage operation. To date $\sim$20% strains have been reported in similar electrochemically activated $\pi-\pi$-stacking polymers [64].

This technology is in an early phase of research. A challenge is that the new molecules are unlikely to achieve the same high conductivity as polypyrrole and polyaniline. Low conductivity

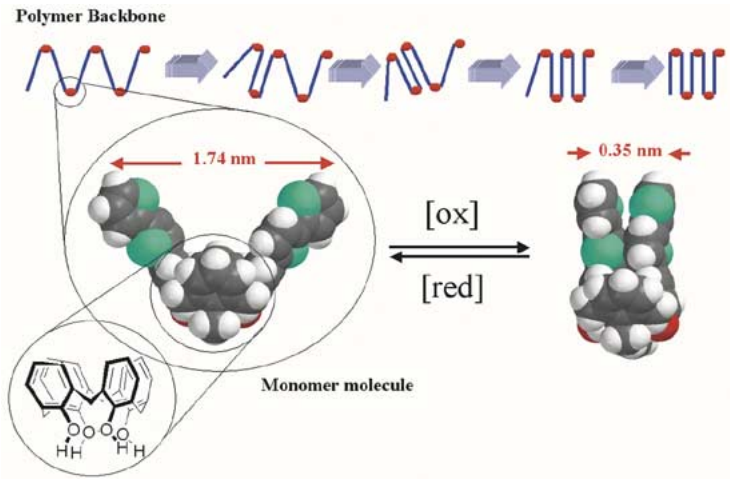

Fig. 6. Schematic of the actuation mechanism of poly(CalixBBT) [64]. The polymer consists of hinge molecules (calix[4]arene) linked by stiff quarterthiophene rods. The polymers are designed such that oxidation of the rods leads to an attractive force between them, resulting in contraction of the polymer.

slows charging and reduces power output [43]. However, conductivity is not as important in these new materials because the number of charges required to achieve displacement is substantially smaller ($\sim$100$\times$). A further challenge is to effectively coordinate molecular motions to create larger scale deformations and forces. More information on this technology is provided in a paper by Swager and Yu in this issue.

Marsella and colleagues achieve actuation by electrochemically switching polymerized cyclooctatetraene and related materials. These materials are predicted to undergo reversible planar to "boat"-shape conformational changes. In theory strains should reach $\sim$6% [67], [68]. It remains to be demonstrated that observed actuation in these materials and in the quarterthiophene-based actuators result directly from conformational changes on the backbone, and are not a result instead of ion and solvent insertion.

3) Photoinduced Mechanical Response in Polymers: Zimmerman and Stille [61] among others have demonstrated that molecular scale activation can be harnessed to actuate bulk materials using photoactivated cis-trans isomerizations. Molecular force probes have been used to directly measure similar cis-trans isomerizations in single molecules [69]. Three percent strains are observed, which is about half of the 7% strain predicted for these azobenzene based oligomers. Fig. 7 depicts the photoactivated conformational changes that are induced in azobenzene containing polymers.

In order to achieve conversion between cis and trans states an activation barrier must be overcome. Absorbed photons provide the energy to overcome this barrier. Most of the input energy is expended in overcoming the barrier rather than in performing mechanical work. Hugel *et al.* [69] estimate a peak efficiency of 10% for azobenzene, which is reduced to $\sim$6% when the photon energies required to both contract and elongate the polymer are included. Observed efficiencies obtained to date are far lower.

The stress can be estimated from the molecular cross-sectional area and the applied force (200 pN typical, no actuation observed above 500 pN), yielding an estimated peak stress of $\sim$1 MPa. If the estimated peak stresses, strains, and efficiencies are to be achieved in bulk materials all molecules must be aligned in the direction of the applied force.

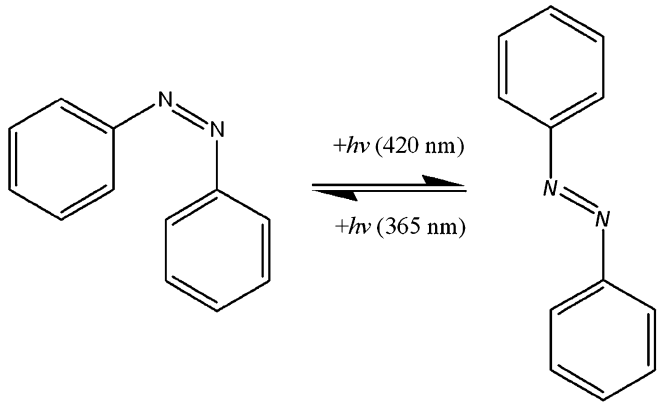

Fig. 7. Schematic of the photoinduced cis (left) to trans conformational change in azobenzene. Monomers containing azobenzene and similar subunits are polymerized to create long actuating molecules [61], [69].

Photoinduced actuation may prove effective for medical applications, micro/nano devices, and perhaps even submersibles tethered to an optical cable.

G. Carbon Nanotube Actuators (Table VI)

Carbon nanotubes (CNTs) are hollow cylinders consisting solely of carbon. These tubes have diameters that are typically 1.2 nm or larger [70], [71]. Their structure is that of a single rolled sheet of graphite that can have lengths on the micrometer scale. These tubes are either conductive or semiconductive, with one-third exhibiting metallic properties [70]. Van der Waal's forces cause the tubes to aggregate in bundles, with bundle diameters of 10 nm being typical in samples used in actuation studies [71]. Multiwall nanotubes are also observed and consist of concentric tubes [70]. Multiwall nanotubes are thought to be less effective actuators because their solvent accessible surface area is typically lower than that of single walled nanotubes, even in bundled form. Surface area is important because actuation is associated with the charging of exposed nanotube surfaces. This is achieved by immersing nanotubes in an electrolyte and applying a potential between the nanotubes and a counter electrode. Ions are attracted to the nanotubes, leading to the accumulation of ionic charge at their surfaces, which is balanced by electronic charge within the tubes. The

TABLE VI
CARBON NANOTUBE ACTUATORS [71], [72], [73], [74]

PROPERTY	TYP.	MAX	LIMIT
Strain (%)	0.2	~1	> 1
Stress (MPa)	1	27 ~0.15 % strain	20,000
Work Density (kJ/m^3)	2	40	$3\cdot10^4$
Strain Rate (%/s)	0.6	19	190,000
Power (W/kg)	10	270	10^{10}
Coupling (internal)	0.001		0.43
Efficiency (%)	0.1		> 22
Density (kg/m^3)	230	1000	
Modulus (GPa)	1 paper	10 fiber	640 single tube
Tensile Strength (MPa)	5	> 40	40,000
Cycle Life, 1 Hz, ±0.5 V	33 % reduction in strain over 140 kcycles		
Applied Potential (V)	1	30 fast activation	
Charge Transfer (C/m^3)	$6\cdot10^6$		$\sim10^8$
Conductivity (S/m)	40,000		500,000
Cost (US$/kg)	<< 50,000	500,000	

TABLE VII
IONIC POLYMER METAL COMPOSITES

PROPERTY	MIN.	TYP.	MAX.
Strain (%)		0.5 [82]	3.3 [81]
Stress (MPa)	0.23[90]	3 [86]	15 [84,86]
Work Density (kJ/m^3)			5.5 [81]
Strain Rate (%/s)			3.3 [81]
Power (W/kg)			2.56 [81]
Coupling (%)			3
Efficiency (%)		1.5 [86]	2.9 [86]
Modulus (GPa)	0.05[90]	0.1 [90]	
Density (kg/m^3)		1500 [89]	
Applied Potential (V)	1	1-4	7 [89]
Charge Transfer (C/m^3)		900,000	
Charge Transfer (C/m^2)		900	
Cost (US$/kg) Min est. materials cost w/ Pt electrodes, Max. - [91].		500	100,000

charging leads to a rearrangement of the electronic structure of the nanotubes, and to Coulombic forces, both of which result in dimensional changes. In tube bundles some slip may also occur between the outer charged tubes and inner isolated layers [74]. For moderate to large levels of charging the Coulombic forces dominate, resulting in a parabolic relationship between strain and applied potential [71]. The parabolic relationship is lost at high potentials as ions and solvent in solution begin to exchange electrons with the nanotubes, discharging the double layer and thereby limiting the maximum achievable strains. Strains reach between 0.1% and approximately 1% [71]. Although these strains are small compared to those obtained in dielectric elastomers and even ferroelectric polymers, individual carbon nanotubes feature high elastic moduli (640 GPa) and enormous tensile strengths ($\gg$1 GPa), potentially enabling unprecendented work densities to be achieved ($\sim$200 MJ/m^3).

As in conducting polymers, it is the rate at which charge can be injected which determines the strain rate. The enormous internal surface area provided by the carbon nanotubes results in an enormous capacitance (26 F/g) [72]. Given the applied potentials are on the order of 1 V, the resulting charge transfer is $\sim$26 C/g. Once again the reduction of cell internal resistance is critical to achieving high strain rates [43]. Speeds of ion transport within the carbon nanotube papers and fibers may also limit rate. As in conducting polymers, very high rates will be observed in nanoscale devices. As an extreme example, in a short 1.2 nm diameter nanotube immersed in aqueous potassium chloride electrolyte that is separated from another tube by 10 nm, the RC charging time constant is estimated to be on the order of 0.1 ns, and the diffusion time constant is approximately 1 ns. In large devices these rates drop off rapidly, with timescales on the order of seconds being typical in actuators that are approximately 30 μm thick. In composite carbon nanotube fibers in which a binder such as polyvinylalcohol is present [75] rates are much slower still due to the slow rate of ion transport within the binder [74]. If large nanotube actuated devices are to be practical, microstructuring of the materials will be necessary to ensure that electrode spacings, diffusion distances and conduction paths are minimized [43]. Resistance compensation techniques can be employed to improve actuation rates, at the expense of some efficiency [53], [73]. Such techniques have enabled response times of several milliseconds to be achieved and effective strain rates of 19%/s [74].

1) Materials: Carbon nanotubes can be synthesized by laser ablation, arc discharge, chemical vapor deposition, and deposition from low cost precursors [70]. They are commercially available from many sources. CNT papers and fibers are filtered [71] or spun [75] from large numbers of nanotubes suspended in solution.

2) Limitations: The small to moderate strains require some mechanical amplification for most applications. The electromechanical coupling is poor, requiring substantial energy recovery to achieve reasonable efficiencies. The material cost is currently very high ($\sim$\$100/g). Films and fibers still exhibit bulk mechanical properties that fall far short of those of single nanotubes. This actuator technology is very new, however, and progress on many of these issues is expected to be rapid. Newly reported porous metals and oxides appear to be actuated using mechanisms similar to those in CNTs, and also promise to provide relatively high performance [76].

H. Ionic Polymer/Metal Composites (IPMCs) (Table VII)

An IPMC consists of a polymer electrolyte sandwiched between two thin metal layers [77]–[86].[5] Deflection of the layered structure toward one of the metal electrodes occurs as a result of a field induced change in ion concentration, which attracts water molecules (or other solvents) to one side of the polymer. The nonuniform distribution of water produces swelling of one side

[5]Biomimetic Products Inc. and EAMEX Corp., http://www.biomimetic.com/, http://www.environmental-robots.com/, http://www.eamex.co.jp/index_e.html

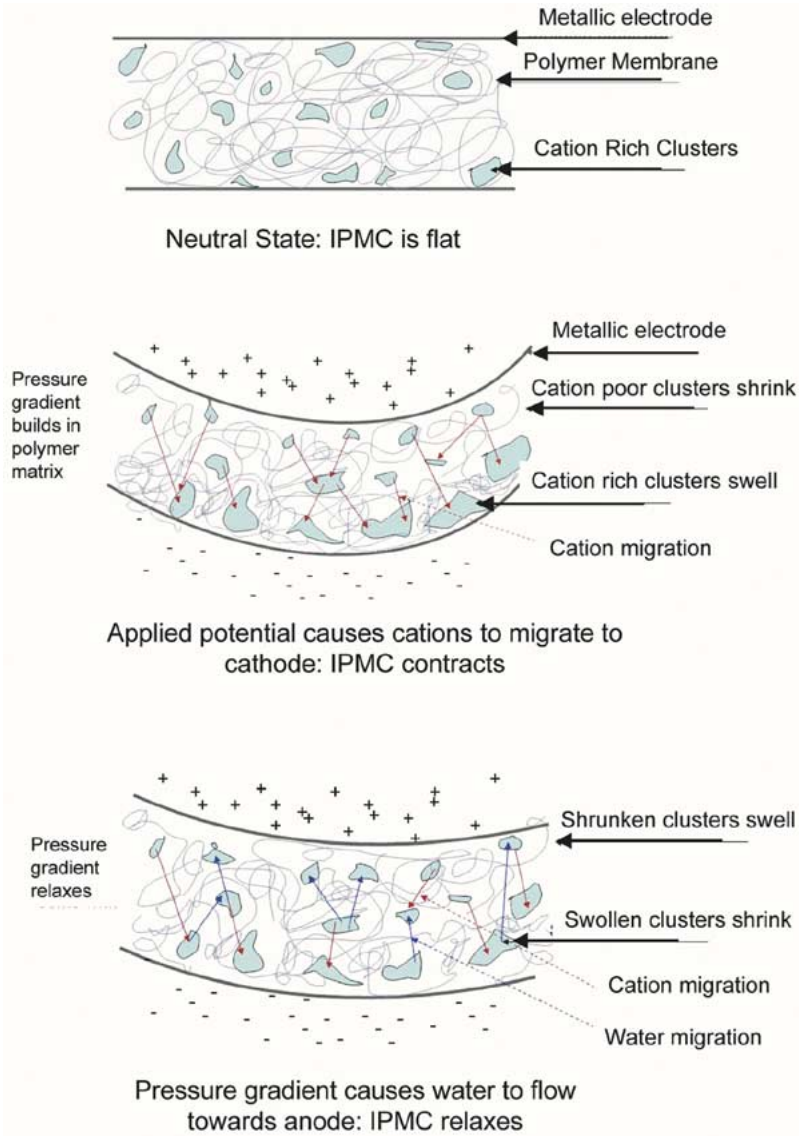

Fig. 8. Mechanisms of IPMC actuation. The clusters shown above represent hydrophilic regions containing ions and solvent.

of the actuator and contraction of the other, generating torque on the member and a bending motion.

1) Mechanisms: The ionic polymers used in IPMC actuators are generally negatively charged, with this charge being balanced by mobile cations. There are also pockets of solvent (e.g., water) in which the cations are dissolved. When an electric field is applied across a strip of IPMC, the ions redistribute themselves, resulting in the formation of two thin boundary layers—a cation-poor layer on the anode side of the polymer and a cation-rich layer on the cathode side, as depicted in Fig. 8. As cations travel to the cathode side of the IPMC, water follows, causing the hydrophilic expansion. The strain in the cathode layer induces stresses in the rest of the polymer matrix, resulting in a fast bending motion toward the anode [80], [81]. After this immediate response, the pressure from the strained polymer matrix causes water to diffuse out of the cation-rich areas, resulting in a slow relaxation toward the cathode [80], [81]. Reversing the applied potential inverts the bending and the subsequent relaxation. The degree of actuation exhibited is dependent on the type of polymer, the counter ion used, and amount of water present [80] as well as the quality of metallization [83], the thickness [77], and the surface area of the polymer membrane [84].

2) Materials and Fabrication: Typical polymers are perfluorinated alkenes with anionic-group-terminated side chains, such as Nafion [77], [79] and Flemion [80] or styrene/divinylbenzene-based polymers with ionic groups substituted from phenyl rings [77]–[79]. Styrene/divinylbenzene based polymers tend to be highly cross-linked, so their potential as an actuator is severely limited by their stiffness. The perfluorinated alkenes form a more flexible matrix [77]–[79]. In the IPMC matrix, the backbone of the polymer is hydrophobic while the anionic sidechains are hydrophilic. This causes the polymers to make clusters of concentrated anions, neutralizing cations and water within the polymer network [79]–[83].

In most cases, a commercially available polymer membrane is used for the polymer layer. These membranes are not manufactured specifically for IPMCs, however, and limit the choice of film thicknesses [77]. Kim and Shahinpoor have addressed this problem by solution recasting Nafion to thicknesses ranging from 30 μm to 2 mm [77]. Noh *et al.* also used a recasting

method to make Nafion membranes with much higher surface area [84].

Both sides of the polymer membrane are loaded with metal nanoparticles and then metal plated [77]–[85]. The nanoparticles balance the charging that occurs in the boundary layers of the polymer, while the metal plating increases surface conductivity and reduces solvent loss upon actuation [86]. The metal nanoparticles are usually 3–10 nm in diameter and are distributed in a 10–20 μm deep layer at both surfaces. This is often done by allowing the polymer to soak in a solution containing a metal salt, such as $Pt(NH_3)_4HCl$, so the metal ions can diffuse into the polymer. The polymer is then treated with a reducing agent, such as $LiBH_4$ or $NaBH_4$, to metalize. The primary reaction for platinum IPMCs is as follows [77]–[79], [82]–[85]:

$$LiBH_4 + 4[Pt(NH_3)_4]^{2+} + 8OH^- \Rightarrow 4Pt^o + 16NH_3 + LiBO_2 + 6H_2O. \quad (5)$$

This metallization process is expensive. Shahinpoor and Kim have shown that the cost can be reduced by physically loading the metal particles into the polymer [79]. The electrode layer can then be deposited onto the surfaces. IPMCs manufactured in this way have shown comparable properties to chemically loaded IPMCs, at 1/10 of the manufacturing cost [79].

After the metal particles have been incorporated into the polymer, a metal coating (usually 1–5 μm thick) is deposited [79]. This plating involves reduction of a metal salt, but instead of impregnating the metal into the polymer the reaction coats the surface of the composite. Electrode materials that have been successfully used for this process include platinum, palladium, silver, gold, carbon, copper, graphite, and carbon nanotubes [79], [83]. Platinum is most commonly used as it is has the widest potential region over which it is resistant to corrosion, enabling larger deflection and higher work density. The metal electrode reduces the surface-electrode resistance down to as little as 8.6% of its original value [83], enabling higher current densities and faster actuation.

IPMCs are further described in a paper by Paquette and Kim in this issue, and more details on the manufacturing of IPMCs are available in a recently written review [86]. Samples are now commercially available.

A number of swimming and flapping applications of IPMCs have been reported, representing preliminary uses of polymer artificial muscle technology for hydrodynamic propulsion [87], [88].

I. Thermally Activated Shape Memory Alloys (SMAs) (Table VIII)

Over a century after Joule's discovery of the equivalence of energy and heat the shape memory effect was reported by Chang and Read [93]. They observed that an alloy of gold and copper returns to the same shape if heated after deformation. The same effect was later discovered in indium–titanium alloys by Basinski and Christian [89], and nickel–titanium alloys by Buehler *et al.* [92]. These researchers used the term "shape memory effect" (SMA) to describe the phenomena. Of all the SMAs, nickel–titanium (NiTi) alloys (better known as Nitinol) are the most extensively studied [95]. NiTi fibers and springs have often been studied and used as artificial muscles [91], [96], [98], [101], [102] because of their relative nontoxicity, reasonable cost, and an electrical resistivity that easily lends itself to Joule heating (passing of an electrical current to generate heat).

TABLE VIII
THERMAL SHAPE MEMORY ALLOYS [2]

PROPERTY	MIN.	TYP.	MAX.
Strain (%)		5	8
Stress (MPa)			200
Work Density (kJ/m^3)		1,000	10,000
Strain Rate (%/s)		300	
Power (W/kg)		1,000	>50,000
Life (cycles) at a amplitude strain of:	300 ~5 %		10^7 ~0.5 %
Efficiency (%)			< 5
Modulus (GPa)	20		83
Tensile Strength (MPa)		1,000	
Density (kg/m^3)		6,450	
Applied Potential (V)		4	
Conductivity (S/cm)		12500	14250
Cost (US$/kg)		300	

1) Mechanism: Martensitic transformations are at the heart of the shape memory effect as shown by Otsuka and Shimizu [104]. Martensitic transformations were discovered by the metallurgist Adolf Martens in steels [105]. It was found that the transformation from the high-temperature, body-centered cubic lattice austenitic phase to the low temperature, face-centered tetragonal lattice takes place without atomic diffusion. Martensitic transformations are phase changes that occur as a displacitive, lattice-distortive, first order diffusionless athermal transformations. In NiTi alloys with a surplus of nickel or with nickel partly replaced with a third element, a two-stage martensitic transformation may occur. The intermediate phase has a rhombohedral crystal structure.

In most NiTi alloys the shape memory effect is only observed when an external stress is applied. In the martensitic phase the alloy has a twinned martensite that can be easily deformed as it de-twins. As it is heated it returns to its parent austenitic phase, which is a highly ordered state, and the alloy retrieves a well defined high-temperature shape.

NiTi alloys may also exhibit a two-way shape memory effect (TWSM) first observed by Delaey *et al.* in 1975 and by which the alloy will exhibit the shape memory effect without an external stress [94]. In the two-way shape memory effect NiTi alloys also have a "remembered" state at low temperature as well as all the intermediate shapes between the high temperature and low temperature. The origin of TWSM is stress-biased martensite and it can only be obtained by special conditioning involving thermomechanical treatment.

The contraction time of NiTi is governed by the speed at which the martensitic to austenitic phase transformation occurs and hence by the electrical power when electrical Joule heating is used. By using very large current pulses this contraction time can be reduced to several milliseconds [101]. The NiTi contraction and expansion cycles are mainly limited by the time

required for NiTi to cool and return to its lower temperature shape. The cooling time is governed by thermal diffusion and convection. Factors such as heat capacity and latent heat involved in the phase transformation between the austenitic and martensitic phases must be considered when designing an actuator. Use of water cooling and nucleate boiling can dramatically reduce cooling time, enabling millisecond response times [101].

2) Features [89]–[105]: Shape memory alloys can exert very large forces per unit area (exceeding 200 MPa), operate at very high strain rates (300%/s) and undergo relatively large deformations (>5% for polycrystalline NiTi fibers). The peak energy density (10^7 J·m^{-3}) and power per unit mass (50 kW·kg^{-1}) of these actuators is unmatched.

3) Limitations: SMAs have several characteristics that impede their use as muscle-like actuators. One of them is the difficulty of controlling the length of NiTi fibers as they undergo a phase transformation. The change in length is observed over a narrow temperature range and a significant hysteresis is observed between the martensitic to austenitic and austenitic to martensitic phases. The phase transformation temperatures vary more or less linearly with stress and the cycling characteristics also change if only partial transformations occur. All of these factors must be modeled appropriately when NiTi fibers are used in a servo-actuator.

NiTi actuators also have a limited cycle life. At very large strains their shape memory effect degrades significantly, from millions of cycles at 0.5% strains to a few hundred cycles at strains of 5% [95] depending on the alloy and conditioning. Their usage is also limited by the low efficiency of NiTi fibers in converting electrical energy to mechanical work which is found to be 5% in the best case (including recovery of energy from heat, [103]) and is usually much lower.

4) Materials: Nickel–titanium shape memory alloys are commercially available from several sources including Shape Memory Applications Inc. (http://www.sma-inc.com)

5) Applications: NiTi wires, tubes, and components are widely used in medical applications due to their super-elasticity, a property related to the memory effect. Little use is made of the actuation properties.

J. Ferromagnetic Shape Memory Alloys (FSMAs) (Table IX)

Interest in the conversion of magnetic energy to mechanical work dates back to Joule and his discovery of the magnetostrictive effect, in which he measured microstrain in a nickel rod placed in a magnetic field. Little advance had been made in the capabilities of magnetic actuators until work on lanthanide metals led to the discovery and development of giant magnetostrictive materials. These materials continue to be a viable actuator choice to this day, with the benchmark, the commercially available alloy Terfenol-D ($Tb_{0.3}Dy_{0.7}Fe_2$) obtaining typical strains of 0.2% at fields of 2000 kA/m against 20 MPa stresses and with frequency responses in the kilohertz range. More information on these materials is available from reviews on giant magnetostrictive materials by Clark [106] and Jiles [107], and in commercial specifications.[6] Modeling [108], and samples of characterization and device research [109]–[111], are also found in the literature.

[6]http://www.etrema-usa.com

TABLE IX
FERROMAGNETIC SHAPE MEMORY ALLOYS [115], [116], [119]

PROPERTY	MIN.	TYP.	MAX.
Strain (%)		6	10
Stress (MPa)	0.005	1	9
Work Density (kJ/m^3)	< 1 including coils	100 without coils	
Strain Rate (%/s)		10,000 (5% @ 1kHz)	
Coupling (%)		75	100 theorized
Density (kg/m^3)		8000	
Modulus (GPa)	0.02 mixed variant	2	90
Saturation Magnetization, μ_0M (T)		0.6	
Cost (US$/kg)		10,000	

While the giant magnetostrictive materials provide a small stroke actuator technology, discovery of the shape memory effect in a magnetic material led to the development of ferromagnetic shape memory alloys (FSMAs). Following the discovery of the thermally induced martensitic transformation below the Curie temperature in the ferromagnetic Ni_2MnGa Heusler alloy in 1995 [112], it was postulated that large strains could also be obtained magnetically. Scarcely a year later, strains of 0.2% were observed in a single crystal of the same composition upon the rotation of a magnetic (H) field of order 600 kA/m [113], surpassing the strains achieved with Terfenol-D. Further investigation into the effects of varying the atomic composition of the alloy on the martensitic transition and Curie temperatures [114] along with better characterization techniques have since led to measurements of 6% [115] and even 10% [116] linear strains under applied fields of the same order of magnitude. These strains may be obtained against stresses of order 1 MPa and with response times in the milliseconds at room temperature.

1) Mechanism: The mechanism involves transitions between variants of the tetragonal martensite phase that are formed upon cooling from the cubic austenite phase. The martensite unit cell is shorter than the cubic cell in one axis (typically referred to as the c-axis) and longer in the other two. Cooling under zero load results in the presence of all three possible anisotropic variants organized into domains. The martensite unit cell is magnetically easy along its shortest (c) axis and may be transformed into one of its orthogonally aligned neighbor variants mechanically or magnetically. Typically, samples are prestressed in compression to align the sample along the shorter c-axis. Upon the application of a magnetic field orthogonal to the direction of stress, regions of the magnetically favored variant nucleate and grow. These regions may be monitored by the appearance of twin boundaries, which are observed to move along the sample as the intensity of the field is increased [117], [118]. The magnitude of the bias or prestress is important as an insufficient stress will leave the sample uncompressed and an

overstress will block the transition. Blocking stresses between 2 and 9 MPa have been reported [115]. Following the removal of the field, stresses above 0.5 MPa are sufficient to return the sample to original dimensions [115].

2) Modeling: Modeling of the FSMA effect is complicated by the many responses a material may exhibit under a large magnetic field. O'Handley first discussed this phenomenon in terms of the anisotropy energy, or energy required to change the magnetization of the material away from its easy axis [120]. Simple rotation of the magnetization and subsequent crystalline distortion is the basis for magnetostriction and has led to some confusion within the FSMA literature. In the case of FSMA materials, however, the anisotropy energy is relatively large, resulting in the favorable transformation of the unit cell into an orthogonally aligned variant. This changes the crystal lattice but keeps the magnetization in the easy axis. Further development of the model [121] along with experimental results have led to the following expression for strain, ε, as a function of magnetic field H

$$\varepsilon(H) = [2 \cdot K_u \cdot h \cdot (1 - h/2) - \sigma \cdot \varepsilon_o]/(C_{\text{eff}} \varepsilon_o) \quad (6)$$

where K_u is the uniaxial anisotropy constant, typically of order $1 \cdot 10^5$ J/m^3, $h = (M_s \cdot \text{Ho}/(2 \cdot \underline{K_u})$ is the ratio of magnetic saturation multiplied by the applied field to twice the anisotropy constant, σ is the uniaxial applied stress, ε_o is the maximum transformation strain (taken to be 0.06 in [115]), and C_{eff} is the effective modulus of the twinned state, taken to be 20 GPa [115].

A simpler mechanistic approach was proposed by Tickle *et al.* [122], in which it was postulated that the easy axis remain fixed to the crystal lattice and the strain response governed by the volume fraction of each of the three variants. This approach led to linear models of the average magnetization and the average unaxial strain $\langle \varepsilon \rangle$

$$\langle \varepsilon \cdot \hat{e}_1 \rangle = \varepsilon_2 \cdot \xi_1 + \varepsilon_1 \cdot (\xi_2 + \xi_3) \quad (7)$$

where ε_1 and ε_2 are the strains associated with the long and short axes, $\hat{e}_1$, and $\hat{e}_2$, of the martensite, taken to be 0.013 and -0.048, respectively, in the reference, and ξ_i is the volume fraction of the variant with its easy axis in the i direction. Note that the model is oriented along the $\hat{e}_1$ axis. By combining the volume fraction strain model with the magnetic saturation, qualitative predictions of strain and strain direction are achieved.

3) Materials: Single crystal Ni_2MnGa and slight variations are used. Other ferromagnetic alloys (such as Fe-Pd and Fe-Ni-Co-Ti) show similar effects, but smaller strains. Polycrystalline Ni_2MnGa also exhibits FSMA behavior, but at reduced strains due to alignment and loading within a matrix [123].

4) Features: Large strains ($\sim$10%) are obtained in stiff (up to 90 GPa modulus) crystalline alloy systems. Fast response ($\sim$1 kHz) and reasonable cycle life ($\sim 5 \times 10^7$ cycles) are also observed in the commercially available materials.[7]

5) Limitations: High intensity magnetic fields are required ($\sim$600 kA/m) and the fields need to be applied orthogonal to stroke direction, adding challenge to the device design. Although the stresses against which the actuators will work are relatively large (several megapascals), this stress value does not account for the cross-sectional area needed to generate the magnetic fields. For example, in Adaptamat Ltd. products the active material produces 1 MPa stresses, but once the coils necessary to produce field are added, the effective stress drops to $<$20 kPa. The presence of the coils also drops the work density to 0.12 kJ$\cdot$m^{-3}. Furthermore, repeated actuation requires a compressive restoring force (e.g., a spring). Finally, modulus appears to change tremendously via mechanical alignment of the twin variants in the martensite phase (dropping to 0.02 GPa as the sample transitions from multiple variants to one single variant [115]). The compliance may result in low resonance frequencies.

6) Temperature: Operation must be near the martensitic transformation temperature (ranging between 200–350 K) and below Curie temperature (325–350 K), both of which vary with composition [114].

7) Applications: Linear motors are available from Adaptamat Ltd. operating with strains $\sim$3% at 2 MPa (not including the electromagnets).

8) Potential: Observed strain has reached the known theoretical limit. However, new passive shape memory effect discoveries may lead to higher strains [124].

III. Case Studies

Two case studies that represent promising applications of artificial muscle technology are presented. Both applications are targeted at AUVs, where size, power consumption, and cost need to be minimized. The examples represent situations that are very commonly encountered in engineering design across all applications. In the first case, varying propeller blade camber using artificial muscle is proposed. In the second, amplification of propeller thrust by the generation of unsteady flow is presented. In the first application rates are relatively slow—the challenge is to incorporate the actuator within the space allotted. In the second, specific power and fuel efficiency become critical.

A. Case Study: Variable Camber Propeller

Controllable pitch propellers are employed in situations where vessels operate under a range of flow conditions. The hypothesis is that AUVs could benefit tremendously from the added efficiency, maneuverability, and the potentially lower noise emissions afforded by variable shape propellers [87]. The objective is to find an alternative to the gearing mechanisms employed in larger vessels, in which force and displacement are projected down a rotating shaft to the blades. We seek to determine, based on the force and displacement requirements, whether any of the artificial muscle technologies are suitable for this application.

The target vehicle for variable camber is the Expendable, Mobile Antisubmarine Warfare Training Target (EMATT) from Sippecan Inc, Marion, MA. The expendable nature of the vehicle makes cost a key consideration. (Details on this application are provided in an accompanying article by Madden in this issue, and in [125].)

1) Specifications: This design is for a propeller blade that has a span (length) of 50 mm, a chord (width) of 25 mm, and an average thickness of 6 mm. The last 10 mm of the chord at

[7]http://www.adaptamat.com

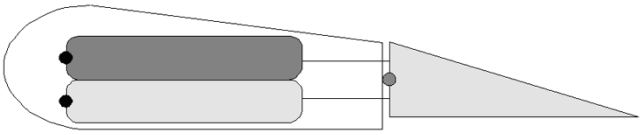

Fig. 9. Lever arm design for creating variable camber. The triangular tail section pivots about a joint (gray circle). Torque is applied to the trailing edge section via an antagonistic actuator pair (ovals) coupled via tendons.

the trailing edge can be pivoted so as to enable variable camber. Fig. 9 shows the approximate geometry. The angle of the trailing edge is to be adjusted up or down by 22° under a force of up to 3.5 N. The dimensions and blade loading are estimated based on the specifications, size and speed of the EMATT vehicle. The numbers are not exact, but allow a demonstration of the methodology used in actuator selection.

In order to simplify the calculations the unknown distribution of the force is applied at a single point at 3 mm from the trailing edge, or, equivalently, 7 mm from the pivot point. The force of 3.5 N generates a torque of $T = 25$ mN·m about the pivot. If the angle of deflection is $\theta = 45°$, the work that must be done is $W = T \cdot \theta = (25\ \text{mN m}) \times (\pi/4) = 19$ mJ.

In the EMATT vehicle a dc electrical power source composed of 15 DD size lithium primary batteries is capable of delivering up to 9 A at battery voltages. The vehicle mission lifetime is up to ten hours, over which time up to 10 000 actuation cycles will be performed. Typically these vehicles are expendable, as their name implies, so the mission length represents the total lifetime. Minimizing cost is also be important in these AUVs.

Will the actuator fit within the space? Ideally the mechanism employed will fit within a propeller blade. The nonpivoting portion of each blade has a volume of 6 mm × 15 mm × 50 mm = 4.5×10^{-6} m^3. Given the required work, the minimum work density in order to fit the actuator within the propeller volume is approximately 4.2 kJ·m^{-3}. In fact the work density will need to be at least double this value, or >8 kJ·m^{-3} as otherwise no space is allotted for structural elements, power delivery, encapsulation and any desired sensors. The higher the work density of an actuator material is above this value, the smaller the volume that will be required and the easier will be the fit.

The data in Table X suggest that silicone dielectric elastomers and IPMCs do not currently demonstrate sufficient work density for this application. Inclusion of activation coils needed to generate magnetic field in the energy density calculation eliminates the ferromagnetic SMAs. Note that the lower energy densities of these technologies could be compensated for by using multiple actuator strokes to deflect the trailing edge (e.g., using a ratchet mechanism). However, this adds to the complexity and cost of the device.

2) Mechanical Amplification: The linear actuators discussed range in strain from less than 1% to more than 100%, and the stresses from the low kPa range up to 200 MPa. If the force divided by the cross-sectional area of the blade ($3.5\ \text{N}/(50\ \text{mm} \times 6\ \text{mm}) = 12$ kPa) is less than the stress that an actuator is capable of generating, then no amplification of the force is required. Furthermore, if the strain multiplied by the length of the actuator is roughly equal to the required displacement of the trailing edge (=3 mm × sin(45°)/15 mm = 14% strain), then little or no amplification of the strain is required, simplifying design and fabrication. (In this estimate it is assumed that some mechanical amplification is occurring, with the actuators attaching at points 3 mm above and below the joint, and the actuators running the length of the leading section. This amplification will roughly require a doubling of the actuator stress.) The ideal actuator will feature both high strain and high stress. Low values of either indicate a need for mechanical amplification, and the smaller the values the greater the amplification.

TABLE X
COMPARISON OF WORK DENSITIES AND STRAINS

MATERIAL	WORK DENSITY (kJ/m^3)	STRAIN (%)
Skeletal Muscle	< 40	20
IPMC	5.5	0.5
Dielectric Elastomer (Silicone)	10 #	120 max
Field Driven Liquid Crystal Elastomer [39]	20 #	2
Carbon Nanotubes	40	0.2
Thermal Liquid Crystal	56	19 - 45
Ferromagnetic SMA	100*	6
Conducting Polymer	100	2
Dielectric Elastomer (VHB)	150 #	380 max
Ferroelectric Polymers	320 #	3.5
Thermal SMA	1000	5

Represents internal energy density that must be coupled to the load. Coupling will reduce energy density by a factor of 2 at least.
* Does not include the coil volume.

Based on strains, as listed in Table X, carbon nanotube actuators are excluded from initial consideration as a mechanical amplification factor of 70 is needed. As carbon nanotube energy densities get closer to the upper bound of 30 MJ/m^3 (determined by the properties of individual tubes) the relatively small strains should eventually be compensated for by the minimal actuator volume requirements, making mechanical amplification worthwhile.

3) Example—Thermal LCE Actuation: To make these considerations more concrete, consider designing a liquid crystal elastomer-based actuator for this application. The highest strain thermal liquid crystal elastomer reported in the literature [34] deforms by 40% under a load of 140 kPa yielding a work density of 56 kJ/m^3, well over the required work density.

As a simple design exercise, we can model a lever arm that pulls around the pivot, as depicted in Fig. 9, deflecting the trailing edge segment. If the muscle attachment points are a distance of 2 mm from the pivot (in the vertical direction), the muscles must exert a force F to balance the torques

$$F = \frac{(3.5\ \text{N})(7\ \text{mm})}{(2\ \text{mm})} = 12.5\ \text{N}. \tag{8}$$

The liquid crystal elastomer can exert a stress of 140 kPa and thus the cross-sectional area needed to generate a force of 12.5 N is

$$A = \frac{12.5\ \text{N}}{140\ \text{kPa}} = 90 \times 10^{-6}\ \text{m}^2 \tag{9}$$

or, if the width of the muscle is taken to be the length of the blade (50 mm), the thickness h of the muscle must be

$$h = \frac{A}{L} = 1.8\,\text{mm}. \tag{10}$$

The muscle length that is needed to get a 45° rotation of the trailing edge is roughly $\Delta x = 2\,\text{mm} \times \sin(45°) = 1.4\,\text{mm}$. If the total strain of the actuator is 40%, then an actuator length of only 3.5 mm is needed to give the required deflection. The calculations show that an LCE actuator could be used for this application based on these considerations alone.

In changing camber, a 1 s response time is ample. All the actuators presented can reach this target. However, thermally activated liquid crystal elastomers, in which heat must be transferred to or from the polymer, will need to be laminated into layers on the order of 100 μm in thickness, and have a mechanism for transferring heat to and from each layer [refer to (3)]. Increasing temperature of the elastomer is relatively easy as this can be done via resistive heating. Removing heat will be more challenging, likely requiring a copper heat sinks or even water cooling.

Conducting polymers must also be laminated in order to achieve the required response time [43]. The actuator material thickness cannot exceed ~30 μm if the actuator is to respond within 1 s—otherwise diffusion of ions into the polymer will be too slow. A laminated or porous structure is required. Other actuators will require laminated structures, but for different reasons. In dielectric elastomers and relaxor ferroelectrics thin layers (~100 μm thick) are used to keep voltages in the low kilovolt range. Thermally activated shape memory alloys employ wires that are ~100 μm in diameter. Larger diameters would reduce resistance and may require excessive currents during Joule heating. Like LCEs, SMAs will require cooling.

4) Voltage Requirements: Ferroelectric polymers, dielectric elastomers, and, to a lesser degree, field driven liquid crystal elastomers all require high fields in order to produce substantial displacement. In order to prevent voltages from being excessive, these materials will need to be layered. One hundred μm thick layers require 1.5 kV in ferroelectric polymers and dielectric elastomers, and as low as 150 V in LCEs. For optimum performance, these layers should also be prestrained, adding to complexity of assembly. Note that for the ferroelectrics and dielectric elastomers in particular, additional cost and space will be needed for dc–dc power converters [125].

5) Catch State: In varying camber it is anticipated that one angle of deflection may prove optimal over long periods of time. Thus, it is best if no power input is required to maintain the desired position. Thermally activated SMAs and LCEs generally require continued heat input in order to hold a fixed position, and thus consume substantial power even when no work is being performed. As a result, SMAs and thermal LCEs are not suited for steady state applications.

6) Continuously Variable Positioning: Actuation of SMAs (including ferromagnetics) involves phase changes. It is easy to run these phase changes to completion each time actuation is performed, but it is a challenge to control the phases such that an intermediate state is reliably reached [2]. For this reason SMAs and thermal liquid crystals are again not appropriate for the variable camber application.

TABLE XI
ACTUATOR SELECTION: VARIABLE CAMBER

MATERIAL	ACCEPT?	POTENTIAL PROBLEMS
Skeletal Muscle	No	Not an engineering material (yet).
Ferromagnetic SMA	No	Coil volume prohibitive. Binary positioning only.
Dielectric Elastomer (Silicone)	o.k.	High voltage requirement & encapsulation. Energy density only just sufficient.
Carbon Nanotubes	No	Strain too small.
IPMC	No	Work density too low.
Thermal Liquid Crystal Elastomer	No	Heat exchange, control & no catch state.
Dielectric Elastomer (VHB)	Yes	High voltage & encapsulation
Conducting Polymer	Yes	Lamination, encapsulation & amplification.
Ferroelectric Polymers	Yes	High voltage & encapsulation.
Thermal SMA	No	Binary positioning only, no catch state.
Field Driven Liquid Crystal [36]	No	Not enough work density. Mechanical & voltage amplification required.

Having considered energy density, mechanical amplification, voltage, controllability, and energy expenditure, each actuator technology may be accepted or rejected, as presented in Table XI.

Table XI lists candidate actuator technologies that are potentially suitable for the variable camber application. Of these VHB-based dielectric elastomers, ferroelectric polymers, and conducting polymers are most attractive on a work density basis. Field actuated liquid crystal elastomers are eliminated from consideration because although their work density exceeds the 8 kJ/m^3 required, the useable work density will be at least a factor of four lower. The listed work density is internal energy, or which at most half can be extracted, bringing the effective work density to $<$10 kJ/m^3. Furthermore, the actuation mechanism will likely require antagonistic pairs of actuators, each of which actuate for only half of the stroke, thereby reducing the effective work density to $<$5 kJ/m^3, below the desired 8 kJ/m^3.

Encapsulation of the actuators to separate them from the saline environment is a technological challenge remaining for all the technologies. Conversion of the available power to kilovolt level potentials will be required in order to operate dielectric elastomers and relaxor ferroelectric polymers. The relatively low degree of electromagnetic coupling in conducting polymers will make energy recovery circuitry necessary in cases where camber is being varied often or continuously as otherwise substantial energy may be required, significantly shortening the life of the power source.

Three technologies are promising for the variable camber application, namely dielectric elastomers, conducting polymers, and ferroelectric polymers.

B. Case Study 2: Unsteady Flow Hydrodynamics

Flapping and rolling motions in a critical range of frequencies to foils and propellers may increase thrust for a given propeller rotation rate (e.g., see Triantafyllou *et al.* in this issue). Lower

TABLE XII
ACTUATOR SUMMARY

Actuator	Advantages	Disadvantages	Comments
Mammalian Skeletal Muscle	Large strains (20 %). Moderate Stress (350 kPa blocking). Variable stiffness. High energy fuel (20-40 MJ/kg). Efficient (~ 40 %). Good work density (< 40 kJ/kg). High cycle life (by regeneration).	Not yet an engineering material. Narrow temperature range of operation. No catch state (expends energy to maintain a force w/o moving, unlike mollusk muscle).	Incredibly elegant mechanism that is a challenge to emulate. Muscle is a 3D nanofabricated system with integrated sensors, energy delivery, waste/heat removal, local energy supply and repair mechanisms.
Dielectric Elastomers	Large strain (20% - 380 %). Moderate stress (several MPa peak). Large work density (10k to 3.4 MJ/m^3). Moderate to high bandwidth (10 Hz to > 1 kHz). Low cost. Low current. Good electromechanical coupling & efficiency (> 15 % typical, 90 % max).	High voltages (> 1 kV) and fields (~150 MV/m). Typically requires DC-DC converters. Compliant ($E \sim 1$ MPa). Pre-stretching mechanisms currently add substantial mass and volume, reducing actual work density and stress.	Potential to lower fields using high dielectric materials. Small devices are favored for high frequency operation eg. MEMS. (due to the more efficient heat transfer which prevents thermal degradation, and the higher resonant frequencies). Starting materials are readily available.
Relaxor Ferroelectric Polymers	Moderate strain (< 7 %). High stress (45 MPa blocking). Very high work density (up to 1 MJ/m^3 internal strain). Stiff (400 MPa). Strong coupling (0.4) & efficiency. Low current.	High voltages (typically > 1kV) and fields (~150 MV/m). Typically need DC-DC converters. Synthesis of typical materials involves environmentally regulated substances. Cycle life is unclear & may be limited by electrode fatigue and dissipation. Limited temperature range.	Lower voltages and fields are being achieved using new high dielectric composites. Small devices are favored for high frequency operation eg. MEMS. Unique combination of high stiffness, moderate strain & reasonable efficiency.
Liquid Crystal Elastomers	Large strains in thermally induced materials (45%). Moderate strains in field induced materials (2-4 %). High coupling (75%) in electrical materials.	Subject to creep. Thermal versions are slow unless very thin or photoactivated. High fields (1-25 MV/m). Low efficiency in thermal materials.	New material with much promise and much characterization to be done. Photo-activation has been achieved.
Conducting Polymers	High stress (34 MPa max, 5 MPa typical). Moderate strain (~ 2 %). Low voltage (~ 2 V). High work density (100 kJ/m^3). Stiff polymers (~ 1 GPa).	Low electromechanical coupling. Currently slow (several hertz maximum to obtain full strain). Typically needs encapsulation.	Promising for low voltage applications. Speed and power will improve dramatically at small scales.
Molecular Actuators	Large strain (20 %). Moderate to high stress (> 1 MPa). Low voltage (2 V). High work density (> 100 kJ/m^3)	Currently slow. Need encapsulation.	Great promise of overcoming many of the shortcomings of conducting polymer actuators, but still very early in development.
Carbon Nanotubes	High stress (> 10 MPa). Low voltage (2 V). Very large operating temperature range.	Small strain (0.2 % typical). Currently has low coupling. Materials are presently expensive.	Great potential as bulk materials approach properties of individual nanotubes.
Ionic Polymer Metal Composites (IPMC)	Low Voltage (< 10 V). Large displacement (mechanical amplification built into the structure).	Low coupling and efficiency. Usually no catch state (consumes energy in holding a position). Requires encapsulation.	IPMC driven toys and demonstration kits are available.
Thermally Activated Shape Memory Alloys	Very high stress (200 MPa). Unmatched specific power (> 100 kW/kg). Moderate to large strain (1-8 %). Low voltage (actual voltage depends on wiring). Great work density (> 1 MJ/m^3)	Difficult to control (usually run between fully contracted and fully extended but not between). Large currents and low efficiencies (<5%). Cycle life is very short at large strain amplitudes.	Readily available. Generally thought of as slow, but can achieve millisecond response times using short high current pulses and water cooling.
Ferromagnetic Shape Memory Alloys	High stress (< 9 MPa). High frequency (> 100 Hz). Moderate strain (up to 10%). High coupling (75%).	Bulky magnets are required which greatly reduce the work density. Costly single crystal materials.	Operates in compression and thus needs a restoring force. Displacement is typically all or nothing, as intermediate states are difficult to reach reproducibly. Commercially available.

rotation rates can thus be used for a given thrust level, which has implications for noise emission [87].

Can the artificial muscle technologies meet the demands of this high power application?

The Remus AUV[8] is chosen as an example platform for application of novel propulsion concepts. Remus has been

[8]http://www.hydroidinc.com/

selected by the U.S. Navy for performing very shallow water mine counter measures (VSW-MCM).

1) Rate: The Remus propeller runs at ∼25 Hz. To create optimum unsteady flow conditions, the blades must then flap at >50 Hz. This bandwidth requirement immediately eliminates thermally activated LCEs, IPMCs, and conducting polymers as candidate materials. As discussed above, it should be possible to drive these materials up to kilohertz frequencies by modifying their geometries, but current demonstrations operate at only several hertz. Based on speed of response alone the candidate actuator technologies are reduced to thermal SMA, ferroelectric polymers, ferromagnetic SMAs, silicone elastomers, carbon nanotubes, and field driven liquid crystal elastomers.

2) Cycle Life: A Remus mission lasts up to 22 h, which corresponds to ∼4 million actuator cycles. This cycle number is approaching or exceeding the limits so far measured for most technologies. In order to achieve this cycle number, the amplitude of actuation will need to be reduced to <3% in thermally activated SMAs. Actuators will generally need to be replaced following each mission.

3) Input Energy and Power: Remus is equipped with a 1 kW·h lithium ion cell. Thermally activated SMAs and LCEs as well as conducting polymers, carbon nanotubes, and IPMCs all operate at low voltages and are thus well matched to the lithium ion cell. The low electromechanical coupling of these actuators however results in input electrical powers that are ∼100× greater than the work output resulting in a need for currents that are ∼100× larger than are needed for an actuator with perfect coupling. The battery thus drains ∼100× faster, and 100× more power is demanded. The battery mass required in order to employ the flapping foil actuators would need to be about 30 times greater than it is at present to generate the required currents. Rates of energy expenditure can be reduced by recovering stored energy in some actuators, thereby improving efficiency. However, high currents will still be needed, which will result in more battery mass being required due to the relatively low power to mass of battery technologies. Therefore these low voltage actuator technologies are not currently practical for such high bandwidth, high power applications when only finite energy and power are available.

In ferroelectrics and dielectric elastomers, dc to dc converters will be required to convert battery voltages to kilovolt levels. It remains to be determined how much space this will occupy over and above the cell. Energy recovery circuitry may also be needed to obtain reasonable efficiencies and mission lengths in these actuators, further increasing the volume required.

Ferromagnetic SMAs can easily achieve the required bandwidths and the coils needed to produce the required fields can operate at the available voltages. The low energy density of ferromagnetic SMAs (once coils are included) may be a limiting factor.

4) Results: Based on preliminary design considerations, ferroelectric polymers, dielectric elastomers, and ferromagnetic SMAs all merit consideration for generating unsteady flow in Remus. These technologies all operate effectively at high bandwidths. Cycle life, encapsulation, and voltage conversion are among the challenges that may prevent or impede the use of these actuators.

IV. Discussion

Table XII presents a summary of the properties of the actuator technologies discussed.

Acknowledgment

J. D. W. Madden is very grateful to F. Tschurtschenthaler at the University of British Columbia, Dr. R. Kornbluh at SRI, and Professor K. Kim at the University of Nevada for their valuable comments and discussion. Dr. P. Bandyopadhyay and Dr. H. Bright of the U.S. Office of Naval Research provided the vision and motivation for this review.

References

[1] J. Hollerbach, I. Hunter, and J. Ballantyne, "A comparative analysis of actuator technologies for robotics," in *The Robotics Review*, O. Khatib, J. Craig, and T. Lozano-Perez, Eds. Cambridge, MA: MIT Press, 1992, vol. 2, pp. 299–342.

[2] I. Hunter and S. Lafontaine, "A comparison of muscle with artificial actuators," in *Tech. Dig. IEEE Solid State Sensors Actuators Workshop*, 1992, pp. 178–185.

[3] Y. Bar-Cohen, Ed., *Electro Active Polymers (EAP) as Artificial Muscles: Reality Potential and Challenges*. Bellingham, WA: SPIE Press, 2001.

[4] M. Zupan, M. F. Ashby, and N. A. Fleck, "Actuator classification and selection," *Adv. Eng. Mater.*, vol. 4, pp. 993–940, 2002.

[5] A. Lendlein and R. Langer, "Biodegradable, elastic shape-memory polymers for potential biomedical applications," *Science*, vol. 296, no. 5573, pp. 1673–1676, May 31, 2002.

[6] K. J. Kim, J. Caligiuri, K. Choe, and M. Shahinpoor, "Contraction/elongation behavior of cation-modified polyacrylonitrile fibers," in *Proc. SPIE Smart Structures and Materials 2003: Electroactive Polymer Actuators and Devices (EAPAD)*, vol. 5051, Y. Bar-Cohen, Ed., 2003, pp. 207–213.

[7] R. Full and K. Meijer, "Metrics of natural muscle," in *Electro Active Polymers (EAP) as Artificial Muscles: Reality Potential and Challenges*, Y. Bar-Cohen, Ed: SPIE Press, 2001, pp. 67–83.

[8] W. C. Roentgen, *About the Changes in Shape and Volume of Dielectrics Caused by Electricity*. ser. Annual Physics and Chemistry Series, G. Wiedemann, Ed. Leipzig, Germany: J. A. Barth, 1980, vol. 11, sec. III, pp. 771–786. German.

[9] R. Kornbluh, R. Pelrine, Q. Pei, S. Oh, and J. Joseph, "Ultrahigh strain response of field-actuated elastomeric polymers," in *Proc. SPIE Smart Structure and Materials 2000: Electroactive Polymer Actuators and Devices*, vol. 3987, 2000, pp. 51–64.

[10] Q. Pei, M. A. Rosenthal, R. Pelrine, S. Stanford, and R. D. Kornbluh, "Multifunctional electroelastomer roll actuators and their application for biomimetic walking robots," in *Proc. SPIE Smart Structures and Materials 2003: Electroactive Polymer Actuators and Devices (EAPAD)*, vol. 5051, Y. Bar-Cohen, Ed., pp. 281–290.

[11] S. Ashley, "Artificial muscles," *Sci. Amer.*, pp. 52–59, Oct. 2003.

[12] G. Kofod, "Dielectric elastomer actuators," Ph.D. dissertation, Technical Univ., Denmark, Sept. 2001.

[13] P. Sommer-Larsen, G. Kofod, S. MH, M. Benslimane, and P. Gravesen, "Performance of dielectic elastomer actuators and materials," in *Proc. SPIE Smart Structures and Materials, Electroactive Polymer Actuators and Devices*, vol. 4695, 2002, pp. 158–166.

[14] R. Pelrine, R. Kornbluh, Q. Pei, S. Stanford, S. Oh, and J. Eckerle, "Dielectric elastomer artificial muscle actuators: Toward biomimetic motion," in *Proc. SPIE Smart Structures and Materials, Electroactive Polymer Actuators and Devices*, vol. 4695, 2002, pp. 126–137.

[15] A. Wingert, M. D. Lichter, S. Dubowsky, and M. Hafez, "Hyper-redundant robot manipulators actuated by optimized binary-dielectric polymers," in *Proc. SPIE Smart Structures and Materials 2002: Electroactive Polymer Actuators and Devices (EAPAD)*, vol. 4695, Y. Bar-Cohen, Ed., pp. 415–423.

[16] R. Kornbluh and R. Pelrine, "Application of dielectric EAP actuators," in *Electro Active Polymers (EAP) as Artificial Muscles: Reality Potential and Challenges*, Y. Bar-Cohen, Ed: SPIE Press, 2001, vol. 67–83, pp. 457–495.

[17] R. Kornbluh, private communication, Jan. 2004.

[18] Q. M. Zhang, J. Li, M. Poh, F. Xia, Z.-Y. Cheng, H. Xu, and C. Huang, "An all-organic composite actuator material with a high dielectric constant," *Nature*, vol. 419, pp. 284–287, 2002.

[19] Q. Zhang and J. Scheinbeim, "Electric EAP," in *Electroactive Polymer Actuators as Artificial Muscle*, Y. Bar-Cohen, Ed. Bellingham, WA: SPIE Press, 2001, pp. 89–117.

[20] Q. Zhang, "P(VDF-TrFE)-based electrostrictive Co/Ter-polymers and its device peformance," in *Electroactive Polymer Actuators and Devices*, Y. Bar-Cohen, Ed. Bellingham, WA: SPIE Press, 2001, pp. 106–116.

[21] V. Bharti *et al.*, "High dielectric constant composites based on metallophthalocyanine oligomer and poly(vinylidene fluoride-trifluoroethylene) copolymer," *J. Appl. Polymer Sci.*, vol. 82, pp. 70–75, 2001.

[22] K. Tashiro, S. Nishimura, and M. Kobayashi, "Thermal contraction and ferroelectric phase transition in vinylidene fuoride-trifluoroethylene copolymers. 1. An effect of tensile strength along the chain axis," *Macromolecules*, vol. 21, pp. 2463–2469, 1988. ACS.

[23] Kobayashi, "Semicrystalline ferroelectric fluoropolymers and process for preparing same,", Mar. 2002.

[24] Q. M. Zhang *et al.*, "Electrostrictive poly(vinylidene fluoride-trifluoroethylene) copolymers," *Sensors Actuators A*, vol. 90, pp. 138–147, 2001.

[25] ——, "Poly(vinylidene fluoride-trifluoroethylene) based high performance electroactive polymers," in *Electroactive Polymer Actuators and Devices*, Y. Bar-Cohen *et al.*, Ed. Bellingham, WA: SPIE Press, 2003, pp. 133–142.

[26] F. Xia, H. Li, C. Huang, M. Huang, H. Xu, F. Bauer, Z.-Y. Cheng, and Q. Zhang, "Poly(vinylidene fluoride-trifluoroethylene) based high performance electroactive polymers," in *Proc. SPIE Smart Structures and Materials, Electroactive Polymer Actuators and Devices*, vol. 5051, 2003, pp. 133–142.

[27] P. G. deGennes, T. C. Chung, and A. Petchsux, *Seances Acad. Sci.*, ser. B, 1975, vol. 281, p. 101.

[28] W. Lehmann, L. Hartmann, F. Kremer, P. Stein, H. Finkelmann, H. Kruth, and S. Diele, "Direct and inverse electromechanical effect in ferroelectric liquid crystalline elastomers," *J. Appl. Phys.*, vol. 86, no. 3, pp. 1647–1652, Aug. 1, 1999.

[29] W. Lehmann, H. Skupin, C. Tolksdorf, E. Gebhard, R. Zentel, P. Kruger, M. Losche, and F. Kremer, "Giant lateral electrostriction in ferroelectric liquid-crystalline elastomers," *Nature*, vol. 410, no. 6827, pp. 447–450, Mar. 22, 2001.

[30] N. Leister, W. Lehmann, U. Weber, D. Geschke, F. Kremer, P. Stein, and H. Finkelmann, "Measurement of the pyroelectric response and of the thermal diffusivity of microtomized sections of 'single crystalline' ferroelectric liquid crystalline elastomers," *Liquid Cryst.*, vol. 27, no. 2, pp. 289–297, Feb. 2000.

[31] S. S. Roy, W. Lehmann, E. Gebhard, C. Tolksdorf, R. Zentel, and F. Kremer, "Inverse piezoelectric and electrostrictive response in freely suspended flc elastomer film as detected by interferometric measurements," *Molec. Cryst. Liquid Cryst.*, vol. 375, pp. 253–268, 2002.

[32] D. K. Shenoy, D. L. Thomsen, A. Srinivasan, P. Keller, and B. R. Ratna, "Carbon coated liquid crystal elastomer film for artificial muscle applications," *Sensors Actuators A*, vol. 96, no. 2–3, pp. 184–188, Feb. 28, 2002.

[33] H. Skupin, F. Kremer, S. V. Shilov, P. Stein, and H. Finkelmann, "Time-resolved ftir spectroscopy on structure and mobility of single crystal ferroelectric liquid crystalline elastomers," *Macromolecules*, vol. 32, no. 11, pp. 3746–3752, June 1, 1999.

[34] D. L. Thomsen, P. Keller, J. Naciri, R. Pink, H. Jeon, D. Shenoy, and B. R. Ratna, "Liquid crystal elastomers with mechanical properties of a muscle," *Macromolecules*, vol. 34, no. 17, pp. 5868–5875, Aug. 14, 2001.

[35] J. Naciri, A. Srinivasan, W. C. Sandberg, R. Ramamurti, and B. Ratna, "Nematic liquid crystal elastomers as artificial muscle materials," *IEEE J. Oceanic Eng.*, to be published.

[36] C. H. Huang, Q. Zhang, and A. Jakli, "Nematic anisotropic liquid-crystal gels," *Adv. Functional Mater.*, vol. 13, pp. 525–529, 2003.

[37] H. Finkelmann and M. Shahinpoor, "Electrically-controllable liquid crystal elastomers-graphite composite artificial muscles," in *Proc. SPIE Electroactive Polymers and Devices 2002*, vol. 4695, 2002.

[38] R. H. Baughman, "Conducting polymer artificial muscles," *Synth. Metals*, vol. 78, pp. 339–353, Apr. 15, 1996.

[39] Q. Pei and O. Inganas, "Electrochemical application of the bending beam method. 1. Mass transport and volume changes in polypyrrole during redox," *J. Phys. Chem.*, vol. 96, pp. 10507–10 514, 1992.

[40] *Handbook of Organic and Conductive Molecules and Polymers*, H. S. Nalwa, Ed., Wiley, Chichester, U.K., 1997, pp. 517–594.

[41] T. E. Herod and J. B. Schlenoff, "Doping induced strain in polyaniline: Stretchoelectrochemistry," *Chem. Mater.*, vol. 5, pp. 951–955, 1993.

[42] J. D. Madden, P. G. Madden, P. A. Anquetil, and I. W. Hunter, "Load and time dependence of displacement in a conducting polymer actuator," *Proc. Materials Research Soc.*, vol. 698, pp. 137–144, 2002.

[43] J. D. Madden, P. G. Madden, and I. W. Hunter, "Conducting polymer actuators as engineering materials," in *Proc. SPIE Smart Structures and Materials 2002: Electroactive Polymer Actuators and Devices*, Y. Bar-Cohen, Ed., Bellingham, WA, 2002, pp. 176–190.

[44] A. Mazzoldi, A. Della Santa, and D. De Rossi, "Conducting polymer actuators: Properties and modeling," in *Polymer Sensors and Actuators*, Y. Osada and D. E. De Rossi, Eds. Heidelberg, Germany: Springer-Verlag, 1999.

[45] J. D. Madden, "Conducting polymer actuators," Ph.D. dissertation, Massachusetts Institute of Technology, Cambridge, 2000.

[46] J. D. Madden, P. G. Madden, and I. W. Hunter, "Characterization of polypyrrole actuators: Modeling and performance," in *Proc. SPIE 8th Annu. Symp. Smart Structures and Materials: Electroactive Polymer Actuators and Devices*, Y. Bar-Cohen, Ed., Bellingham, WA, 2001, pp. 72–83.

[47] M. Kaneko, M. Fukui, W. Takashima, and K. Kaneto, "Electrolyte and strain dependences of chemomechanical deformation of polyaniline film," *Synth. Metals*, vol. 84, pp. 795–796, 1997.

[48] R. H. Baughman, R. L. Shacklette, and R. L. Elsenbaumer, "Micro electromechanical actuators based on conducting polymers," in *Topics in Molecular Organization and Engineering, Vol. 7: Molecular Electronics*, P. I. Lazarev, Ed. Dordrecht: Kluwer, 1991, p. 267.

[49] J. Ding, L. Liu, G. M. Spinks, D. Zhou, G. G. Wallace, and J. Gillespie, "High performance conducting polymer actuators utilizing a tubular geometry and helical wire interconnects," *Synth. Metals*, vol. 138, no. 3, pp. 391–398, 2003.

[50] K. Kaneto, M. Kaneko, Y. Min, and A. G. MacDiarmid, "Artificial muscle: Electromechanical actuators using polyaniline films synthetic metals," *Synth. Metals*, vol. 71, pp. 2211–2212, 1995.

[51] M. Yamaura, T. Hagiwara, and K. Iwata, "Enhancement of electrical conductivity of polypyrrole film by stretching: Counter ion effect," *Synth. Metals*, vol. 26, pp. 209–224, 1988.

[52] G. Wallace, D. Zhou, J. Ding, B. Xi, P. Innis, J. Mazurkiewicz, G. Spinks, J. Gillespie, D. MacFarlane, S. Forsyth, and M. Forsyth, "Ionic liquids and helical interconnects: Bringing the electronic braille screen closer to reality," in *Proc. SPIE Smart Structures and Materials*, vol. 12, 2003, pp. 468–472. G. M. Spinks, D. Z. Zhou, L. Liu, G. G. Wallace, "The amounts per cycle of polypyrrole electromechanical actuators", *Smart Mater. Structures*.

[53] J. D. Madden, R. A. Cush, T. S. Kanigan, and I. W. Hunter, "Fast contracting polypyrrole actuators," *Synth. Metals*, vol. 113, pp. 185–193, May 2000.

[54] M. Yamaura, T. Hagiwara, and K. Iwata, "Enhancement of electrical conductivity of polypyrrole film by stretching: Counter ion effect," *Synth. Metals*, vol. 26, pp. 209–224, 1988.

[55] R. S. Kohlman and A. J. Epstein, "Insulator-metal transistion and inhomogeneous metallic state in conducting polymers," in *Handbook of Conducting Polymers*, T. A. Skotheim, R. L. Elsenbaumer, and J. R. Reynolds, Eds. New York: Marcel Dekker, 1998, pp. 85–122.

[56] N. Vandesteeg, P. Madden, J. Madden, P. Anquetil, and I. Hunter, "Synthesis and characterization of EDOT-based conducting polymer actuators," in *Proc. SPIE*, vol. 5051, 2003, pp. 349–356.

[57] J. Madden, B. Schmid, R. Botha, M. Hechinger, S. Lafontaine, P. Madden, F. Hover, K. MacLetchie, and I. Hunter, "Application of Polypyrrole Actuators: Feasibility of Variable Camber Foils," *IEEE J. Oceanic Eng.*, vol. 29, no. 3, pp. 738–749, 2004.

[58] J. D. Madden, R. A. Cush, T. S. Kanigan, and I. W. Hunter, "Encapsulated conducting polymer actuators," *Synth. Metals*, vol. 105, pp. 61–64, 1999.

[59] E. Smela, O. Inganäs, and I. Lundström, "Controlled Folding of Micrometer-Size Structures," *Science*, vol. 268, pp. 1735–1738, 1995. E. Smela, "Conjugated polymer actuators for biomedical applications", *Adv. Mater.,* pp. 481–494, vol. 15, 2003.

[60] L. Bay, K. West, P. Sommer-Larsen, S. Skaarup, and M. Benslimane, "A conducting polymer artificial muscle with 12% linear strain," *Adv. Mater.*, vol. 15, pp. 310–313, 2003.

[61] E. K. Zimmermann and J. K. Stille, "Photoresponive polyquinolines," *Macromolecules*, vol. 18, pp. 321–327, 1985.

[62] M. C. Jimenez, C. Dietrich-Buchecker, and J. P. Sauvage, "Toward synthetic molecular muscles," *Angewandte Chemie Int.*, vol. 39, no. 18, pp. 3284–3287, 2000.

[63] T. R. Kelly, H. De Silva, and R. A. Silva, "Unidirectional rotary motion in a molecular system," *Nature*, vol. 401, pp. 150–153, 1999.

[64] P. A. Anquetil, H.-H. Yu, J. D. Madden, P. G. Madden, T. M. Swager, and I. W. Hunter, "Thiophene based molecular actuators," in *SPIE 9th Annu. Symp. Electroactive Materials and Structures*, vol. 4695, San Diego, CA, Mar. 18–21, 2002, pp. 424–434.

[65] R. P. Kingsborough and T. M. Swager, "Polythiophene hybrids of transition-metal bis(salicylidenimine)s: Correlation between structure and electronic properties," *J. Amer. Chem. Soc.*, vol. 121, no. 38, pp. 8825–8834, 1999.

[66] G. Brocks, "π-dimers of oligothiophene cations," *J. Chem. Phys.*, vol. 112, no. 12, pp. 5353–5363, 2000.

[67] M. J. Marsella and R. J. Reid, "Toward molecular muscles: Design and synthesis of an electrically conducting poly[cyclooctatetrathiophene]," *Macromolecules*, vol. 32, pp. 5982–5984, 1999.

[68] M. J. Marsella, R. J. Reid, S. Estassi, and L. S. Wang, "Tetra[2,3-thienylene]: A building block for single-molecule electromechanical actuators," *J. Amer. Chem. Soc.*, vol. 124, no. 42, pp. 12 507–12510, 2002.

[69] T. Hugel, N. B. Holland, A. Cattani, L. Moroder, M. Seitz, and H. E. Gaub, "Single-molecule optomechanical cycle," *Science*, vol. 296, no. 5570, pp. 1103–1106, 2002.

[70] R. Saito, G. Dresselhaus, and M. S. Dresselhaus, *Physical Properties of Carbon Nanotubes*. London, U.K.: Imperial College Press, 1998.

[71] R. H. Baughman, C. Chanxing, A. A. Zakhidov, Z. Iqbal, J. N. Barisci, G. M. Spinks, G. G. Wallace, A. Mazzoldi, D. De Rossi, A. G. Rinzler, O. Jaschinski, S. Roth, and M. Kertesz, "Carbon nanotube actuators," *Science*, vol. 284, pp. 1340–1344, 1999.

[72] J. N. Barisci, G. G. Wallace, and G. Spinks, "Electrochemical characterization of single-walled carbon nanotube electrodes," *J. Electrochem. Soc.*, vol. 147, p. 4580, 2000.

[73] J. N. Barisci, G. M. Spinks, G. G. Wallace, and J. D. Madden, "Increased actuation rate of electromechanical carbon nanotube actuators using potential pulses with resistance compensation," *Smart Mater. Structures*, vol. 12, no. 4, pp. 549–555, 2003.

[74] R. H. Baughman and J. D. Madden, Unpublished results.

[75] A. B. Dalton, S. Collins, J. Razal, E. Munoz, V. H. Ebron, B. G. Kim, J. N. Coleman, J. P. Ferraris, and R. H. Baughman, "Continuous carbon nanotube composite fibers: Properties, potential applications, and problems," *J. Mater. Chem.*, vol. 14, no. 1, 1–3, 2004.

[76] G. Gu, M. Schmid, P.-W. Chiu, A. Minett, J. Fraysee, G.-T. Kim, S. Roth, M. Kozlov, E. Munoz, and R. Baughman, "V_2O_5 nanofiber sheet actuators," *Nature Mater.*, vol. 2, pp. 316–319, 2003.

[77] K. J. Kim and M. Shahinpoor, "Development of three dimensional ionic polymer-metal composites as artificial muscles," *Polymer*, vol. 43, pp. 797–802, 2002.

[78] M. Shahinpoor, "Ionic polymer-conductor composites as biomimetic sensors, robotic actuators and artificial muscles—A review," *Electrochimica Acta*, vol. 48, pp. 2343–2353, 2003.

[79] M. Shahinpoor and K. J. Kim, "A novel physically-loaded and interlocked electrode developed for ionic polymer-metal composites," *Sensors Actuators A*, vol. 96, pp. 125–132, 2002.

[80] S. Nemat-Nasser, "Micromechanics of actuation of ionic polymer-metal composites," *J. Appl. Phys.*, vol. 92, no. 5, pp. 2899–2915, 2002.

[81] S. Nemat-Nasser and Y. X. Wu, "Comparative experimental study of ionic polymer-metal composites with different backbone ionomers and in various cation forms," *J. Appl. Phys.*, vol. 93, no. 9, pp. 5255–5267, 2003.

[82] M. Shahinpoor and K. J. Kim, "Ionic polymer-metal composites—I. Fundamentals," *Smart Mater. Struct.*, vol. 10, pp. 819–833, 2001.

[83] ——, "The effect of surface-electrode resistance on the performance of ionic polymer-metal composites (IMPC) artificial muscles," *Smart Mater. Struct.*, vol. 9, pp. 543–551, 2000.

[84] T. Noh, Y. Tak, J. Nam, and H. Choi, "Electrochemical characterization of polymer actuator with large interfacial area," *Electrochimica Acta*, vol. 47, no. 13/14, pp. 2341–2346, 2002.

[85] M. Shahinpoor, Y. Bar-Cohen, J. Simpson, and J. Smith, "Ionic polymer-metal composites (IPMC's) as biomimetic sensors, actuators and artificial muscles—A review," *Smart Mater. Structures Int. J.*, vol. 7, pp. R15–R30, 1998.

[86] K. Kim and M. Shahinpoor, "Ionic polymer-metal composites: II. Manufacturing techniques," *Smart Mater. Struct.*, vol. 12, pp. 65–79, 2003.

[87] P. R. Bandyopadhyay, "A biomimetic propulsion for active noise control: Experiments," Naval Undersea Warfare Center, NUWC-NPT Tech. Rep. 11 351, Mar. 2002.

[88] M. Mojarrad, "Study of ionic polymeric gels as smart materials and artificial muscles for biomimetic swimming robotic applications," Ph.D. dissertation, Dept. of Mechanical Engineering, Univ. of New Mexico, Albuquerque, Dec. 2001.

[89] Z. S. Basinski and T. Christian, "Experiments on the martensitic transformation in single crystals of indium-thallium alloys," *Acta Metallurgica*, vol. 2, p. 101, 1954.

[90] M. Bergamasco, F. Salsedo, and P. Dario, "A linear SMA motor as direct-drive robotic actuator," in *IEEE Int. Conf. Robotics Automation*, Scottsdale, AZ, May 1989, pp. 618–623.

[91] ——, "Shape memory alloy micro-motors for direct-drive activation of dexterous artificial hands," *Sensors Actuators*, vol. 17, pp. 115–119, 1989.

[92] W. J. Buehler, J. V. Gilfrich, and R. C. Wiley, "Effect of low-temperature phase changes on mechanical properties of alloys near composition tini," *J. Appl. Phys.*, vol. 34, no. 5, pp. 1475–1963, 1963.

[93] L. C. Chang and T. A. Read, "Lastic deformation and diffusionless phase changes in metals—The gold-cadmium beta phase," *Trans. Amer. Inst. Mining Metallurg. Eng.*, vol. 191, no. 1, pp. 47–52, 1951.

[94] L. Delaey and J. Thienel, *Shape Memory Effects in Alloys*, J. Perkins, Ed. New York: Plenum, 1975, pp. 341–350.

[95] H. Funakubo, Ed., *Shape Memory Alloys*. New York: Gordon and Breach, 1987.

[96] S. Hirose, K. Ikuta, and Y. Umetani, "A new design method of servo-actuators based on the shape memory effect," in *Proc. RoManSy'84: 5th CISM-IFToMM Symp. Theory and Practice of Robots and Manipulators*, 1985, pp. 339–349.

[97] S. Hirose, K. Ikuta, and K. Sato, "Development of a shape memory alloy actuator. Improvement of output performance by the introduction of a s-mechanism," *Adv. Robot.*, vol. 3, pp. 89–108, 1989.

[98] D. Homma, Y. Miwa, and N. Iguchi, "Micro robots and micro mechanisms using shape memory alloy," in *3rd Toyota Conf. Integrated Micro Motion Systems: Micromachining, Control and Application*, Nissin, Aichi, Japan, Oct. 22, 1989, pp. 1–21.

[99] I. W. Hunter, "Novel actuators for use in robotics and tele-robotics," NTIS, U.S. Office of Naval Research, 1990.

[100] I. W. Hunter, S. Lafontaine, and J. M. Hollerbach, "Artificial muscle prototype for use in robotic and prosthetic limbs," in *Proc. 16th Can. Medical and Biological Engineering Conf.*, vol. 16, 1990, pp. 35–36.

[101] I. W. Hunter, S. Lafontaine, J. M. Hollerbach, and P. J. Hunter, "Fast reversible NiTi fibers for use in microrobotics," in *Proc. IEEE Micro Electro Mechanical Systems*, vol. 2, 1991, pp. 166–170.

[102] K. Ikuta, "Micro/miniature shape memory alloy actuator," in *Proc. IEEE Micro Electro Mechanical Systems*, vol. 3, 1990, pp. 2156–2161.

[103] P. G. McCormick, "On the practical efficiency of shape memory engines," *Scipta Metallugica*, vol. 21, pp. 99–101, 1987.

[104] K. Otsuka and K. Shimizu, "Memory effect and thermoelastic martensite transformation in CU-AL-NI alloy," *Scripta Metallurgica*, vol. 4, no. 6, pp. 469–1970, 1970.

[105] J. Van Humbeeck, M. Chandrasekaran, and L. Delaey, "Shape memory alloys: Materials in action," in *Endeavour*, 1991, vol. 15, pp. 147–154.

[106] A. E. Clark, *Ferromagnetic Materials*, E. P. Wohlfarth, Ed. Amsterdam, the Netherlands: North-Holland, 1980, vol. 1, p. 531.

[107] D. C. Jiles, "The development of highly magnetostrictive rare earth-iron alloys," *J. Phys. D. Appl. Phys.*, vol. 27, no. 1, pp. 1–11, 1994.

[108] R. C. Smith, M. J. Dapino, and S. Seelecke, "Free energy model for hysteresis in magnetostrictive transducers ," *J. Appl. Phys.*, vol. 93, no. y2003, pp. 458–466, 2003.

[109] H. Janocha, "Application potential of magnetic field driven new actuators," *Sensors Actuators A*, vol. 91, no. 1/2, pp. 126–132, June 2001.

[110] F. Claeyssen, N. Lhermet, R. LeLetty, P. Bouchilloux, and J. Alloys, "Actuators, transducers and motors based on giant magnetostrictive materials," *J. Alloys Compounds*, vol. 258, no. 1/2, pp. 61–73, 1997.

[111] L. Sandlund, M. Fahlander, T. Cedell, A. E. Clark, J. B. Restorff, and M. Wunfogle, "Magnetostriction, elastic-moduli, and coupling factors of composite Terfenol-D," *J. Appl. Phys.*, pt. 2A, vol. 75, pp. 5656–5658, 1994.

[112] V. A. Chernenko, E. Cesari, V. V. Kokorin, and I. N. Vitenko, "The development of new ferromagnetic shape memory alloys in Ni-Mn-Ga system," *Scripta Metallurgica et Materialis*, vol. 33, pp. 1239–1244, 1995.

[113] K. Ullakko, J. K. Huang, C. Kantner, R. C. O'Handley, and V. V. Kokorin, "Large magnetic-field-induced strains in Ni_2MnGa single crystals," *Appl. Phys. Lett.*, vol. 69, pp. 1966–1968, 1996.

[114] A. N. Vasil'ev, A. D. Bozhko, V. V. Khovailo, I. E. Dikshtein, V. G. Shavrov, V. D. Buchelnikov, M. Matsumoto, S. Suzuki, T. Takagi, and J. Tani, "Structural and magnetic phase transitions in shape-memory alloys $Ni_{2+x}Mn_{1-x}Ga$," *Phys. Rev. B*, vol. 59, pp. 1113–1120, 1999.

[115] S. J. Murray, M. Marioni, S. M. Allen, R. C. O'Handley, and T. A. Lograsso, "6% magnetic-field-induced strain by twin-boundary motion in ferromagnetic Ni-Mn-Ga," *Appl. Phys. Lett.*, vol. 77, pp. 886–888, 2000.

[116] A. Sozinov, A. A. Likhachev, N. Lanska, and K. Ullakko, "Giant magnetic-field-induced strain in NiMnGa seven-layered martensitic phase," *Appl. Phys. Lett.*, vol. 80, pp. 1746–1748, 2002.
[117] S. J. Murray, M. A. Marioni, A. M. Kukla, J. Robinson, R. C. O'Handley, and S. M. Allen, "Large field indsuced strain in single crystalline Ni-Mn-Ga ferromagnetic shape memory alloy," *J. Appl. Phys.*, vol. 87, pp. 5774–5776, 2000.
[118] R. Tickle, R. D. James, T. Shield, M. Wuttig, and V. V. Kokorin, "Ferromagnetic shape memory in the NiMnGa system," *IEEE Trans. Magn.*, vol. 35, pp. 4301–4310, 1999.
[119] R. Tickle and R. D. James, "Magnetic and magnetomechanical properties of Ni_2MnGa," *J. Magn. Magn. Mater.*, vol. 195, pp. 627–638, 1999.
[120] R. C. O'Handley, "Model for strain and magnetization in magnetic shape-memory alloys," *J. Appl. Phys.*, vol. 83, pp. 3263–3270, 1998.
[121] R. C. O'Handley, S. J. Murray, M. Marioni, H. Nembach, and S. M. Allen, "Phenomenology of giant magnetic-field-induced strain in ferromagnetic shape-memory materials," *J. Appl. Phys.*, vol. 87, pp. 4712–4717, 2000.
[122] R. Tickle, R. D. James, T. Shield, M. Wuttig, and V. V. Kokorin, "Ferromagnetic shape memory in the NiMnGa system," *IEEE Trans. Magn.*, vol. 35, pp. 4301–4310, 1999.
[123] M. A. Marioni, R. C. O'Handley, and S. M. Allen, "Analytical model for field-induced strain in ferromagnetic shape-memory alloy polycrystals," *J. Appl. Phys.*, vol. 91, pp. 7807–7809, 2002.
[124] C. Jiang, T. Liang, H. Xu, M. Zhang, and G. Wu, "Superhigh strains by variant reorientation in the nonmodulated ferromagnetic NiMnGa alloys," *Appl. Phys. Lett.*, vol. 81, pp. 2818–2820, 2002.
[125] J. Madden, "Actuator selection for variable camber propellers," in *Proc. SPIE 11th Annu. Symp. Smart Structures and Materials: Electroactive Polymer Actuators and Devices*, Y. Bar-Cohen, Ed., Bellingham, WA, 2004, to be published.

John D. W. Madden (M'95) was born in Ottawa, ON, Canada in 1968. He received the B.Sc. degree in physics from the University of British Columbia (UBC), Vancouver, BC, Canada, in 1991, the M.Eng. degree in biomedical engineering from McGill University, Montreal, PQ, Canada, in 1995, and the Ph.D. degree from the BioInstrumentation Laboratory, Massachusetts Institute of Technology, Cambridge, in 2000.

He joined UBC in 2002 and is currently an Assistant Professor of electrical and computer engineering. His research involves fundamental studies and applications of polymer and nanotube actuators and electronic devices.

Nathan A. Vandesteeg was born in St. Paul, MN, in 1979. He received the B.Sc. degree in chemical engineering from Rice University, Houston, TX, in 2001. He is currently pursuing the Ph.D. degree in materials science and engineering at the Massachusetts Institute of Technology (MIT), Cambridge.

At MIT he is also enrolled in the program for polymer science and engineering. He was a Drilling Engineer and Reservoir Engineer at BP Amoco Exploration during his tenure at Rice University. His current research interests are nanoscale smart meaterials from chemical design and synthesis to mechanical characterization.

Mr. Vandesteeg is a member of Tau Beta Pi. He received a graduate research fellowship from the National Science Foundation.

Patrick A. Anquetil was born in Boulogne-Billancourt, France, in 1973. He received the M.Sc. degree in mechanical engineering from the Swiss Federal Institute of Technology, Zurich (ETH Zurich), Switzerland, in 1998. He is currently pursuing the Ph.D. degree at the Massachusetts Institute of Technology (MIT), Cambridge.

He conducted research at Tokyo University under Prof. T. Sato and Prof. A. Stemmer. He is leading the conducting polymer effort at the MIT BioInstrumentation laboratory headed by Prof. I. W. Hunter. His research interests include the discovery and characterization of novel conducting polymer actuators, the development of bioinstrumentation for drug discovery, Raman spectroscopy, and nanotechnology.

Peter G. A. Madden was born in Ottawa, ON, Canada, in 1971. He received the B.A.Sc. degree in engineering physics from the University of British Columbia (UBC), Vancouver, BC, Canada, in 1993, the M.Eng. degree in biomedical engineering from McGill University, Montreal, PQ, Canada, in 1996, and the Ph.D. degree in mechanical engineering from the Massachusetts Institute of Technology, Cambridge, in 2003.

He is currently a Postdoctoral Associate in the Department of Organismic and Evolutionary Biology, Harvard University, Cambridge, MA. His current research is in the area of fish pectoral fin propulsion and maneuvering.

Arash Takshi was born in Tehran, Iran, in 1971. He graduated in electronics from Amir Kabir University of Technology (Tehran Polytechnic) in 1993. He received the M.Sc. degree in analog electronics from Sharif University of Technology, Tehran, in 1996. He is currently pursuing the Ph.D. degree at the University of British Columbia, Vancouver, BC, Canada.

His work involves developing polymer transistors. He was with the Electronic Research Center of Sharif University of Technology as a Junior Electronics Engineer until 1998. He was with Fan Niroo Co. in Iran as Senior Engineer and Head of Control and Instrumentation from 1998 to 2002.

Rachel Z. Pytel received the B.S. degree in chemical engineering from Worcester Polytechnic Institute, Worcester, MA, in 2002. She is currently pursuing the Ph.D. degree in materials science and engineering at the Massachusetts Institute of Technology (MIT), Cambridge.

Her current research focuses on developing and characterizing nanostructured conducting polymer actuators. Her interests include the development of processing techniques for conducting polymer molecules, X-ray scattering, atomic force microscopy, and transmission and scanning electron microscopy.

Serge R. Lafontaine received the B.Sc. degree in physics from the University of Montreal, Montreal, PQ, Canada, and the Ph.D. degree from the Department of Biomedical Engineering, McGill University, Montreal.

He is a scientific consultant whose interest is the development of medical and biomedical instrumentation. He spent two years as Postdoctoral Fellow at the BioInstrumentation Laboratory in mechanical engineering at the Massachusetts Institute of Technology. His main research interests include sensors and actuators including conducting polymers and shape memory alloys, data acquisition and control mainly applied to the development of new devices for the characterization of materials and systems, optics, electronics, and software algorithms. He has developed a wide-field optical imaging system for the quantitative detection of fluorescence in high-throughput massively parallel drug discovery, genetic engineering and diagnostic system and a fully digital imaging and beam control system of an electron microscope. He has participated in the creation of several new businesses including Biotrove Inc. and LifeFX Technologies Inc. As Chief Technology Officer of LifeFX, Inc., he led the research and development of the company's software products. His interest in the future will remain in the startup of new companies and development of commercial products.

Paul Wieringa was born in Owen Sound, ON, Canada, in 1980. He received the bachelor's degree in applied science from the University of British Columbia (UBC), Vancouver, BC, Canada, in 2004.

He has been with Pyng Medical Ltd. and Deco Automotive (Magna subsidiary) as a Junior Engineer. He is currently a Research Assistant at UBC. He plans to pursue research in biomimetic engineering.

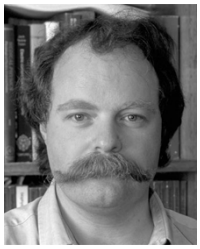

Ian W. Hunter was born in New Zealand in 1953. He received the B.Sc., M.Sc., D.C.P., and Ph.D. degrees in science from the University of Auckland, Auckland, New Zealand in 1974, 1975, 1976, and 1980, respectively.

He was with McGill University, Montreal, PQ, Canada, from 1980 to 1994. He then joined the Faculty of the Massachusetts Institute of Technology, Cambridge, where he presently is the Hatsopoulos Professor of Mechanical Engineering, a Professor of biological engineering, and Head of the BioInstrumentation Lab. His current research interests are microinstrumentation, microfabrication, microrobotics, microsurgical robotics, artificial muscle fibers, laser imaging systems, and instrumentation physics.